Investigating the Climate Impacts of Global Land Cover Change in the Community Climate System Model (CCSM 3.0)

Peter J. Lawrence[1] and Thomas N. Chase[2]

[1] National Center for Atmospheric Research, Boulder, Colorado
[2] Cooperative Institute for Research in Environmental Sciences (CIRES), University of Colorado, Boulder, Colorado

Abstract

Recently, [*Pitman, et al.*, 2009] found a wide range of bio-geophysical climate impacts from historical land cover change when modeled in a suite of current Global Climate Models (GCMs). The bio-geophysical climate impacts of human land cover change however, have been investigated by a wide range of general circulation modeling, regional climate modeling, and observational studies. In this regard the IPCC 4th assessment report specifies radiative cooling of -0.2 W/m^2 as the dominant global impact of human land cover change since 1750, but states this has a low to medium level of scientific understanding. To further contribute to the understanding of the possible climate impacts of anthropogenic land cover change, we have performed a series of land cover change experiments with the Community Land Model (CLM) within the Community Climate System Model (CCSM). To do this we have developed a new set of potential vegetation land surface parameters to represent land cover change in CLM. The new parameters are consistent with the potential vegetation biome mapping of [*Ramankutty and Foley*, 1999], with the Plant Functional Types and plant phenology consistent with the current day MODIS land surface parameters of [*Lawrence and Chase*, 2007]. We found that land cover change in CCSM resulted in widespread regional warming of the near surface atmosphere, but with limited impact on near surface temperatures globally. The experiments also found changes in precipitation, with drier conditions regionally, but with limited impact on average global precipitation. Analysis of the surface fluxes in the CCSM experiments found the current day warming was predominantly driven by changes in surface hydrology through reduced evapo-transpiration and latent heat flux, with the radiative forcing playing a secondary role. We show these finding are supported by a wide range of observational field studies, satellite studies, and regional and global climate modeling studies.

1. Introduction

Recently, [*Pitman, et al.*, 2009] found a wide range of bio-geophysical climate impacts from historical land cover change when modeled in a suite of current Global Climate Models (GCMs) in the Land-Use and Climate, Identification of robust impacts (LUCID) study. The models used in the LUCID study were unable to agree regionally or globally on the climate response of the land cover change, with some of the models having completely opposite changes in surface temperature and latent heat flux associated with the land cover change. The bio-geophysical climate impacts of human land cover change however, have been investigated by a wide range of general circulation modeling, regional climate modeling, and observational studies [*Bonan*, 2008; *Feddema, et al.*, 2005; *Pielke, et al.*, 2002].

While the specific climate impacts found in the modeled and observed land cover change studies varied in strength, [*Bonan*, 2008], [*Feddema, et al.*, 2005] and [*Pielke, et al.*, 2002] all found there were consistent general climate impacts for a specific land cover change in a given geographic locality. In tropical forests they found that land cover change results in warming, with the lower transpiration and canopy evaporation of grasslands and crops resulting in reduced latent heat flux and increased sensible heat flux in response to the increased residual surface energy budget. At higher latitudes they found that land cover change results in cooling due to higher albedo from crops and grasslands that replace darker boreal forests

that mask snow albedo. In mid-latitudes their findings are mixed with the albedo forcing competing against the hydrological forcing for a given land cover change.

The tropical warming and high latitude cooling response to land cover change also can be found through out the literature. The tropical warming is supported by studies from [*Feddema, et al.*, 2005], [*Chase, et al.*, 1996], [*Pielke*, 2001], [*Niyogi, et al.*, 2002], and others that found tropical and temperate deforestation can result in warming of 1-2^{O} C regionally through reduced evapo-transpiration resulting in increased sensible heat flux. In the GCM experiments of these studies the reduced evapo-transpiration was found to impact tropical convection and precipitation, with impacts on monsoon systems, as well as on extra-tropical circulation through tele-connected changes in tropical divergence. The high latitude cooling is supported by studies from [*Oleson, et al.*, 2004], [*Bala, et al.*, 2007], [*Brovkin, et al.*, 1999], [*Betts, et al.*, 2001], and others, that found land cover change results in surface temperature cooling of 1-2^{O} C regionally, principally through increased albedo associated with replacing mid-latitude needleleaf and broadleaf forests with agriculture.

In regard to land cover change, the IPCC 4th assessment report specifies the dominant global impact of human land cover change since 1750 is radiative cooling of -0.2 W/m^2 [*Forster, et al.*, 2007], but suggests there are potentially important non-radiative effects which have low to medium level of scientific understanding. The report states that the radiative cooling is primarily in response to increased surface albedo under current day conditions, but further notes that non-radiative forcings such as changes in evapo-transpiration are important in the tropics where most land use change is currently taking place. [*Bonan*, 2008] suggests that the scientific understanding of land cover change impacts on climate is a necessity for informing climate change mitigation policy.

Recently, we found that the description of plant distributions, seasonal leaf area index phenology, and soil albedo have large impacts on the climate simulated in the Community Land Model (CLM 3.0) and the Community Climate System Model (CCSM 3.0) [*Lawrence and Chase*, 2007]. In addition, we found that improving the global simulation of surface hydrology through vegetation and soils, also has large impacts on the climate simulated in CLM and CCSM [*Lawrence and Chase*, 2009]. In the first study we constrained the current day land surface parameters used in CLM with Moderate Resolution Imaging Spectroradiometer (MODIS) satellite imagery. In the second study we constrained the land surface hydrology to be consistent with global estimates of transpiration, canopy evaporation and soil evaporation from a range of studies.

Simulating these components of the land surface is fundamental in representing land surface energy budgets as well as the surface fluxes of moisture and heat to the atmosphere. These in turn are the bio-geophysical basis for the climate impacts found from land cover change by [*Bonan*, 2008], [*Feddema, et al.*, 2005] and [*Pielke, et al.*, 2002]. Therefore, to further contribute to the understanding of the possible climate impacts of anthropogenic land cover change, we have performed a series of land cover change experiments with the CLM and CCSM models, using these improved representations of current day vegetation, surface albedo, and surface hydrology.

Our investigations were performed as a series of CCSM climate experiments using CLM global land surface parameters that represent current day vegetation compared to the vegetation conditions that may have existed prior to human disturbance. The current day land cover conditions were derived from the MODIS satellite data as described in [*Lawrence and Chase*, 2007], while the potential vegetation was consistently generated using the historical land use and potential vegetation mapping of [*Ramankutty and Foley*, 1999]. These experiments were performed as both multi-member ensembles with prescribed sea surface temperatures and as longer duration fully coupled experiments.

2. Data and Methods

2.1. Global Land Cover Change Mapping

[*Ramankutty and Foley*, 1999] demonstrated that human disturbance through land use and land cover change has substantially altered the world's natural ecosystems, resulting in landscapes that are widely dominated by cultivation, grazing, pastures and urban development. In their study they suggest around 10% of the Earth surface is directly used for some form of cultivation, and nearly another 50% used for pastures and rangelands. The land cover changes between current day and potential vegetation are shown in the vegetation biome mapping of [*Ramankutty and Foley*, 1999] in *Figure 1*, with the global and regional differences in biome composition in *Table 1*.

The biome changes of *Table 1* show that land cover change resulted in a total increase in land use of 15.5% globally. This is consistent with the land cover change analysis of [*Ramankutty and Foley*, 1999], and [*Hurtt, et al.*, 2006] when pasture transitions are included, but is substantially higher than the 11.6% estimate of [*Findell, et al.*, 2007]. In terms of natural biome conversion, the analysis shows losses were greatest in savannas and grasslands, with the total change in savanna, grasslands and shrublands accounting for nearly half of the land cover conversion at 7.4% of land globally. The next largest losses were in temperate forests which accounted for over a quarter of natural land cover conversion at 4.3% of land globally. The changes in tropical forest were marginally smaller than the temperate forests at 3.6% of land globally. The changes in boreal forests were much smaller than the other biome types at 0.2% of land globally, possibly reflecting their poor suitability for agriculture.

Table 1. Global and Regional Land Cover Change in Biome area as a percentage of land area between Current Day and Potential Vegetation biome maps of [Ramankutty and Foley, 1999].

Biome	All Land	India	Europe	China	Brazil	North America
Trop Evg For	-1.51	-9.13	-0.00	-2.66	-4.06	-
Trop Dec For	-2.07	-31.88	-0.11	-0.80	-11.52	-0.00
Temp Brd Evg	-0.46	-0.27	-0.52	-9.33	-0.07	-0.00
Temp Ndl Evg	-0.78	-0.28	-7.32	-2.68	-	-2.69
Temp Dec For	-1.63	0.00	-20.57	-11.37	-	-1.91
Borl Evg For	-0.10	-0.05	-0.45	-0.01	-	-0.04
Borl Dec For	-0.06	-	-0.26	-0.03	-	-0.00
Mixed Forest	-1.35	-1.19	-6.80	-13.28	-	-2.04
Savanna	-3.04	-2.89	-6.43	-3.19	-17.90	-4.60
Grassland	-2.49	-0.18	-7.42	-3.95	-6.87	-9.11
Dense Shrub	-1.31	-3.98	-1.54	-1.01	-6.65	-0.08
Open Shrub	-0.60	-3.21	-0.42	-0.16	-0.02	-0.46
Tundra	-0.07	-0.04	-0.22	-0.01	-0.00	-0.00
Desert	-0.08	-0.99	-0.00	-0.02	-0.01	-0.00
Land use	+15.54	+54.09	+52.05	+48.52	+47.10	+20.92

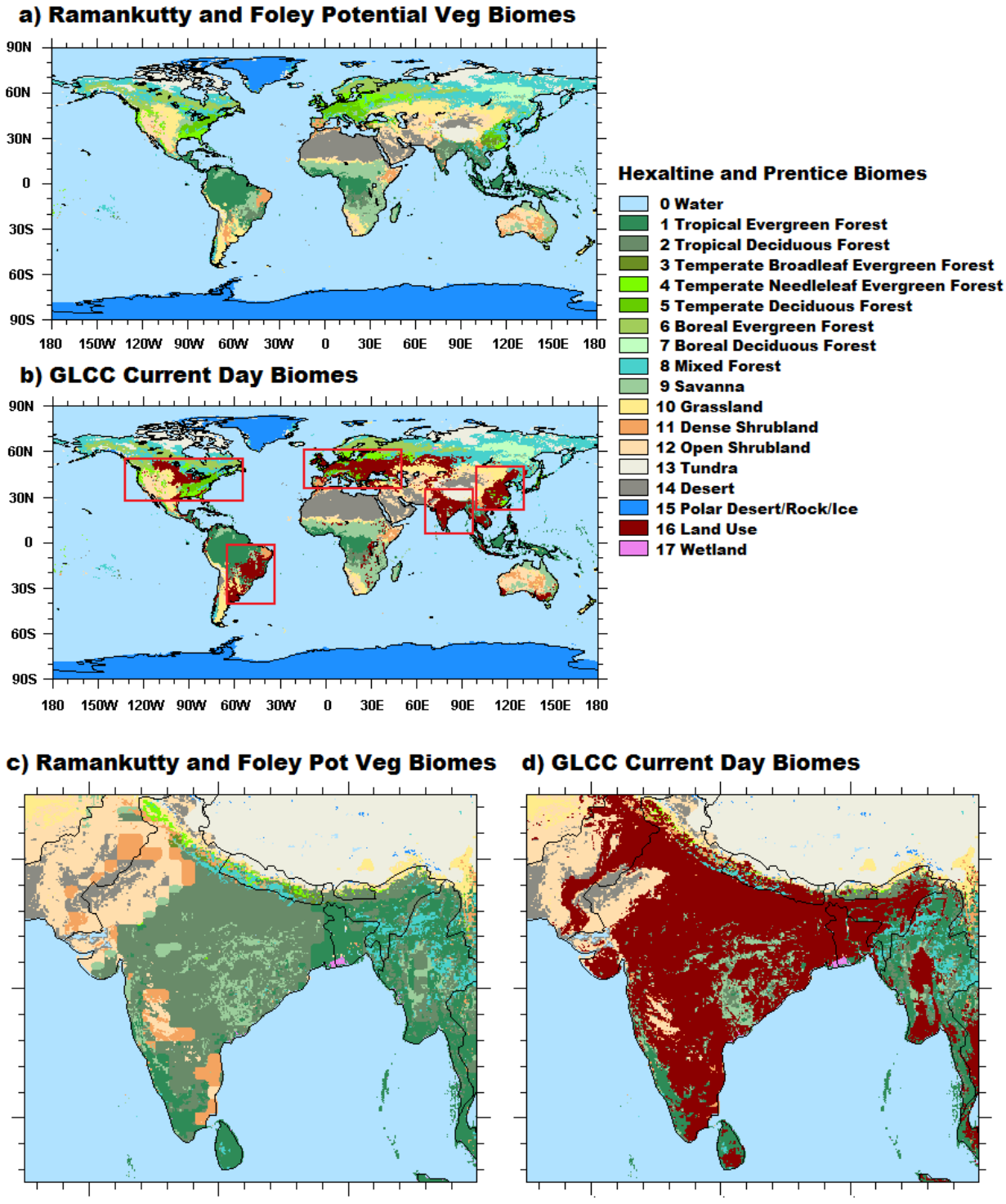

Figure 1. (a) [*Ramankutty and Foley*, 1999] *Global Potential Vegetation;(b) [Loveland, et al., 2000] Global Current Day Biomes; (c) Close in Indian Potential Vegetation; and (d) Close in Indian Current Day Biomes. All maps with the Biome classifications of [Haxeltine and Prentice, 1996]. The Study Regions of North America, Europe, India, China and Brazil are shown in (b).*

The regional analysis shows that the land cover conversion had large differences in extent and the nature of change from region to region. The Indian region had the largest increase in land use at 54.1% of total area. This was followed by the European region at 52.1%, China at 48.5%, Brazil at 47.1% and North America at 20.9%. The natural biomes converted to land use also were different from region to region. In the Indian region, the largest reductions in natural biomes were in tropical deciduous and evergreen forests accounting for 41.1% of land. This was followed by reductions in shublands and savannas accounting for another 10.2% of land.

In the European region, the largest reductions were in temperate and mixed forests accounting for 34.7% of land, with savannas, grasslands and shrublands accounting for another 15.4%. In China, the changes were greatest in temperate and mixed forests accounting for 36.6% of land, with tropical forests, savanna, grasslands and shrublands accounting for another 14.9%. In Brazil the reductions were greatest in savannas at 17.9% of land, followed by tropical forests at 15.6%, and grassland and shrublands at 13.5%. In North America the largest changes were in grasslands at 9.1% of land, followed by temperate and mixed forests at 6.6%, and savannas and shrublands at 5.1%.

2.2. Describing Global Land Cover Change in the Community Land Model (CLM)

The traditional approach to describe the changes in land cover shown by [*Ramankutty and Foley*, 1999] in a climate model would be to change the biomes of the land surface model from those that may have existed prior to human disturbance with those found under current day conditions. The change in biome properties with the two land surface maps would then result in changes in the modeled surface energy and hydrology and therefore fluxes to the atmosphere, with the climate model then simulating climate under the two different land surface representations.

In CLM however, the land surface is represented as a heterogeneous mosaic of Plant Functional Types (PFTs) rather than discrete biomes, complicating the inclusion of land cover change from the traditional biome change approach [*Lawrence and Chase*, 2007]. Despite the added complexity, [*Oleson, et al.*, 2004] suggests that the PFT representation is advantageous as it captures the heterogeneous changes that occur between and within plant biomes, reflecting the geographic dependence of a particular biome on climate, soils and disturbance regime. With the PFT approach the land cover changes can be represented through changes in PFT composition as well as through changes in the individual PFT phenology captured in leaf and stem area indexes (LAI and SAI), canopy height, and indirectly from changes in leaf litter and soil composition represented through background soil color.

Following the CLM land surface scheme, the changes between the two biome maps are represented in this study through a new set of climatological land surface parameters representing the potential vegetation that may have existed prior to human disturbance. The land cover change in CLM is therefore the difference between the potential vegetation parameters and the current day land surface parameters derived from MODIS satellite observation and current day climate described in [*Lawrence and Chase*, 2007] and [*Oleson, et al.*, 2008].

In the absence of global potential vegetation data for PFT contribution, individual PFT phenology and background soil reflectance, these values were spatially extrapolated from the current day remnant natural vegetation to the potential vegetation distribution based on biome type. To be consistent with the current day CLM parameters, the remnant natural vegetation values were taken directly from the MODIS satellite data using the same methods. This resulted in potential vegetation PFT distributions, leaf phenology and soil reflectance that may have existed under current day climatic conditions in line with the bioclimatic modeling of [*Haxeltine and Prentice*, 1996]. The remnant natural vegetation values were spatially extrapolated from current day biome distributions to the potential vegetation biome distributions using the inverse distance weighting methods of [*Shephard*, 1968] at the 0.05 degree resolution of the MODIS data.

To address some of the issues associated with disturbance and degradation in the current day remnant natural vegetation, the MODIS land cover map of [*Friedl, et al.*, 2002] was used as a secondary filter in the extrapolation process. The filter ensured that MODIS data from a current day biome was only used for extrapolation when the current day MODIS IGBP land cover class was consistent with the potential vegetation biome being extrapolated. This filtering mechanism attempted to remove vegetation that may have been degraded between the 1992 current day mapping of [*Loveland, et al.*, 2000] used for current day biome mapping by [*Ramankutty and Foley*, 1999] and the 2001 – 2004 mapping from MODIS satellite imagery used for generating the current day CLM parameters.

The extrapolated potential vegetation land surface properties were processed through the same land surface parameter generation methods as the current day MODIS derived CLM parameters described in [*Lawrence and Chase*, 2007]. This resulted in CLM potential vegetation parameters describing PFTs, monthly LAI and SAI, and soil color. All soil texture and soil slope parameters were left as current day values, neglecting the influence of land use and soil degradation on soil texture and drainage properties. The potential vegetation soil color was generated along with the other PFT parameters to ensure the effective albedo of the current day remnant natural biomes was extrapolated to the potential vegetation biome distributions through background soil reflectivity.

2.3. Experimental Design for CCSM Climate Sensitivity to Land Cover Change

To assess how the land cover changes from potential vegetation to current day impacted the climate simulated in CCSM, we performed a series of climate sensitivity experiments with both sets of land surface parameters. To investigate the robustness of the climate impacts found in CCSM, the experiments were performed firstly using prescribed monthly sea surface temperatures (SSTs) and sea ice, and then repeated using coupled dynamic ocean and sea ice models. All climate simulations were performed with the Community Atmosphere Model (CAM 3.5) as described in [*Neale, et al.*, 2008], at the T42 spectral truncation under current day atmospheric CO_2 concentrations (355 ppm). Issues in evapo-transpiration partition and surface hydrology found in the current release CLM 3.0 by [*Lawrence and Chase*, 2009], [*Oleson, et al.*, 2008] and [*Lawrence, et al.*, 2007], were addressed through using the new CLM SiB surface hydrology described in [*Lawrence and Chase*, 2009].

The prescribed SST experiments were performed using the Data Ocean (DOCN 7.0) model with prescribed monthly SST climatology from 1950 – 2003 cycled annually. The same climatology data was used to prescribe sea ice distributions to the Community Ice CodE (CICE 4.0) model, which calculated surface fluxes from the sea ice to the atmosphere. The prescribed SST experiments were run as an ensemble of three 30 year realizations for each set of land surface parameters to ensure that differences in climate response in CCSM were not dependent on initial conditions. The different initial conditions were set using different years of land initial conditions from a 15 year spin up simulation for each set of land surface parameters. To allow the rest of the model to re-equilibrate to the different land surface conditions, the initial 5 years of each simulation was discarded leaving a total of 75 years of climate for the current day and potential vegetation parameters.

The coupled dynamic ocean experiments used the Parallel Ocean Program (POP 2.0) coupled with the CICE 4.0 model to simulate the oceans and sea ice. The dynamic ocean and sea ice models allowed feedbacks that were not represented in the prescribed SST experiments. The dynamic ocean experiments were run as a single 100 year realization for each set of land surface parameters. Due to the longer spin up time of the ocean model the initial 25 years of each simulation was discarded leaving 75 years of climate for each set of parameters. The longer simulations were done to capture as much inter-annual and inter-decadal climate variability as possible in each of the runs.

Analysis of the mean differences in a range of climate variables was performed through global mapping to show the differences in climatological values for each season for each grid cell and for larger regions. Time series t-tests were performed on each grid cell to identify statistically significant changes for the grid cell and for larger regions between experiments. The mean differences in climate variables also were assessed globally, over all land, and over the five analysis regions of: India, China, North America, Europe and Brazil. The five study regions were selected as they had the largest areas of change in cropping as shown in *Figure 1*.

The regional analyses were performed over all seasons and annually, with the statistical strengths of these relationships assessed through multiple statistical tests. The statistical testing involved a Student's t-test and a Wilcoxon Signed Rank test on each of the time series of seasonal variables to identify statistically significant differences in the experiments. The Wilcoxon Signed Rank test was used following [*von Storch and Zwiers*, 1999], as it is non-parametric and provides insurance against moderate departures from the distribution assumptions required for calculating t-test significance.

3. Land Cover Change in CLM Land Surface Parameters

3.1. Land Cover Change in CLM Plant Functional Types (PFTs)

The differences in PFT composition between current day and potential vegetation CLM parameters are mapped globally in *Figure 2*, and tabulated for all land and the five analysis regions in *Table 2*. Globally the [*Ramankutty and Foley*, 1999] land use was associated with a 9.5% increase in crop PFT and a 0.4% increase in grass PFT contribution. As shown in the global mapping, the increase in cropping followed the distribution of land use found in the global biome mapping (*Figure 2b*). The increases in grass PFTs however, were more complex, with some areas having large increases in grasses and others having large decreases in grasses (*Figure 2d*).

In general the decreases in grass PFTs occurred in areas where natural grasslands and savannas were converted to cropping. This is evident across the North American Prairies, the Russian Steppes, throughout Africa, and the South American Pampas. By contrast the increases in grass PFTs occurred in forested areas or shrublands where the land use primarily involved the creation of pastures for grazing or for forestry. This is evident in eastern North America, western Europe, India, China, South East Asia, eastern Brazil and southern Australia.

Globally the largest decreases in natural PFTs were in tree PFTs. Broadleaf deciduous trees had the largest reduction, in line with the large decreases in deciduous forest and savanna found in the biome analysis. The next largest decrease in trees was in needleleaf trees, reflecting the large decreases in mixed and needleleaf forest biomes. The third largest decrease was in broadleaf evergreen trees associated with the decrease in the tropical evergreen forest biome. Decreases in shrub PFTs were substantially smaller than tree PFTs, reflecting the smaller losses in shrubland biomes and the low vegetation density found in shrublands. The global mapping of tree and shrub PFTs changes also shows the larger tree loss (*Figure 2a* and *b*).

The regional analysis supported the PFT changes found in the global analysis and mapping. India had the largest increase in crop PFT, followed by Europe, and China. North America however, had a larger increase in crop PFT than Brazil, reversing the biome land use order. In India, Europe, China and Brazil land use increases were all associated with increases in grass PFTs, while in North America land use resulted in a decrease of grasses. This reflected the competing impacts of grassland conversion to crops against the creation of pasture for grazing from other PFTs. In North America the conversion of the Prairies to crops out weighed the creation of pasture in the east. While in the other regions the pasture creation out weighed grassland conversion.

In India the loss of natural PFTs was dominated by decreases in broadleaf deciduous trees, associated with the loss of the tropical deciduous forest biome. This was followed by the loss of broadleaf evergreen trees and shrub PFTs. In Europe the loss of natural PFTs also was dominated by broadleaf deciduous trees, but here needleleaf trees made a large contribution reflecting the loss of mixed and needleleaf forest biomes. In China the loss of natural PFTs was evenly split between broadleaf deciduous trees and needleleaf trees with other PFTs having smaller decreases.

In Brazil the loss of natural PFTs was largest in broadleaf evergreen trees, followed closely by the decrease in broadleaf deciduous trees and shrub PFTs. In North America the losses in natural PFTs were evenly split between grasses, needleleaf trees and broadleaf deciduous trees.

Table 2. Global and Regional Land Cover Change in CLM Plant Functional Type (PFT) percentage composition between Current Day and Potential Vegetation parameters.*

PFT	All Land	India	Europe	China	Brazil	North America
B	-0.35	+0.51	-0.31	-0.21	-0.24	-0.60
NEM	-1.72	-0.54	-11.63	-15.26	-	-4.58
NEB	-0.30	-0.02	-1.86	-0.10	-	-0.37
NDB	0.00	-	-	-	-	-
BET	-1.59	-4.28	-	-0.27	-5.59	-
BEM	-0.22	-0.89	-0.11	-0.47	-1.96	-0.00
BDT	-1.75	-29.24	-	-0.30	-6.10	-0.00
BDM	-2.17	-5.24	-18.03	-15.21	-1.01	-4.95
BDB	-0.25	-0.01	-1.88	-0.44	-	-0.31
SEM	-0.18	-0.00	-0.35	-	-0.18	-0.02
SDM	-1.34	-4.60	-2.51	-0.76	-4.87	-0.61
SDB	-0.02	-0.00	-0.04	-0.04	-	-0.03
GA3	+0.01	-0.01	+0.71	-0.16	-	-0.02
GC3	+0.01	+0.18	+5.76	+6.70	+3.81	-4.79
GC4	+0.35	+7.22	+0.10	+5.46	+6.60	-0.50
C	+9.50	+36.89	+30.18	+21.05	+9.56	+16.80

** Plant Functional Types are: B, bare; NEM, needleleaf evergreen temperate tree; NEB, needleleaf evergreen boreal tree; NDB, needleleaf deciduous boreal tree; BET, broadleaf evergreen tropical tree; BEM, broadleaf evergreen temperate tree; BDT, broadleaf deciduous tropical tree; BDM, broadleaf deciduous temperature tree; BDB, broadleaf deciduous boreal tree; SEM, evergreen temperate shrub; SDM, deciduous temperate shrub; SDB, deciduous boreal shrub; GA3, c3 grass arctic; GC3, c3 grass non-arctic; GC4, c4 grass; and C, crop.*

Finally, there was a current day decrease in global bare soil associated with irrigation in areas such as the Indus valley, Eurasia, and the North American mid west (*not mapped*). There also were decreases in bare ground in rain fed areas where shrublands have been replaced by cropping and pastures such as South America and southern Australia. These changes correspond well with the high bare soil fractions found in grassland, shrubland and desert biomes compared to land use.

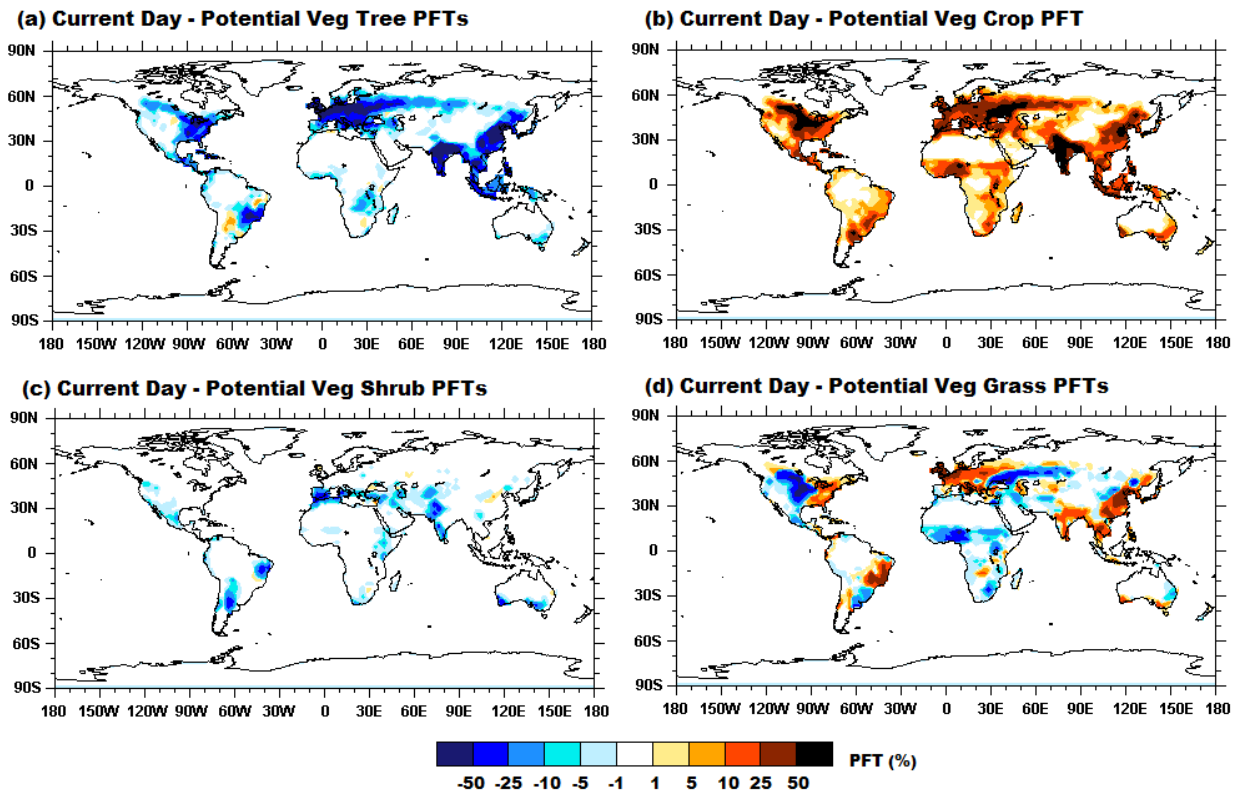

Figure 2. Land cover change in CLM Plant Functional Types (PFTs) between Current Day and Potential Vegetation Parameters.

3.2. Land Cover Change in CLM Leaf Area Index (LAI)

Land cover change between the potential vegetation and current day CLM parameters are globally mapped for seasonal differences in total combined PFT LAI in *Figure 3*, and tabulated for all land and the five analysis regions in *Table 3*. Over all land, the maps and table both show the current day parameters had substantially lower LAI for all seasons, with the largest decreases in boreal summer (JJA) and autumn (SON). The regional LAI analysis shows that all regions had decreases in LAI with the largest decreases in the Indian region. In India the LAI decreases were larger in the post-monsoon and early dry seasons (SON and DJF), and smaller in the late dry and monsoon seasons (MAM and JJA).

China had the next largest decrease in LAI, with larger decreases in summer (JJA) and smaller decreases in winter (DJF). The European region had the third largest decrease, again with the biggest decrease in summer and smallest decrease winter. The Brazilian region had substantially smaller decreases in LAI than the first three regions, with the largest decreases in the dry seasons (JJA and SON). North America had the smallest decrease in LAI with the decreases largest in summer (JJA) and smallest in winter (JJA).

The global maps of seasonal differences in LAI show the land cover changes in CLM LAI had the same general spatial distribution as the change in PFTs, with the current day values lower for all seasons (*Figure 3*). There are a number of areas where the current day parameters have higher LAI than the potential vegetation parameters. In general, these areas corresponded to sparse shrublands and grasslands in the potential vegetation biome map that are used for agriculture in the current day, reflecting the differences in LAI found between grassland, shrubland and desert biomes compared to land use. In the

upper mid-west of North America and over the Indus valley the higher current day LAI also corresponds with widespread irrigation.

Table 3. Global and Regional Land Cover Change in CLM Leaf Area Index (LAI) between Current Day and Potential Vegetation parameters.

Season	All Land	India	Europe	China	Brazil	North America
DJF	-0.07	-0.63	-0.23	-0.29	-0.09	-0.07
MAM	-0.06	-0.45	-0.23	-0.32	-0.11	-0.12
JJA	-0.09	-0.53	-0.49	-0.44	-0.17	-0.16
SON	-0.09	-0.70	-0.35	-0.37	-0.17	-0.11
Annual	-0.08	-0.58	-0.33	-0.36	-0.14	-0.12

The global LAI maps also reflect the seasonal changes found in the All Land and regional LAI analyses and in the biome analysis. In North America, Europe through the Eurasian Steppes, and in China, the decreases in LAI are largest in boreal summer (JJA), with the smallest decreases in boreal winter (DJF). In India and South East Asia the decreases in LAI are largest in the post monsoon and early dry seasons (SON and DJF), and smaller in the pre-monsoon and early monsoon seasons (MAM and JJA). The other major decreases in LAI found in eastern Brazil and south eastern Australia are present all year round with slightly larger changes in the austral winter (JJA) than in the austral summer (DJF).

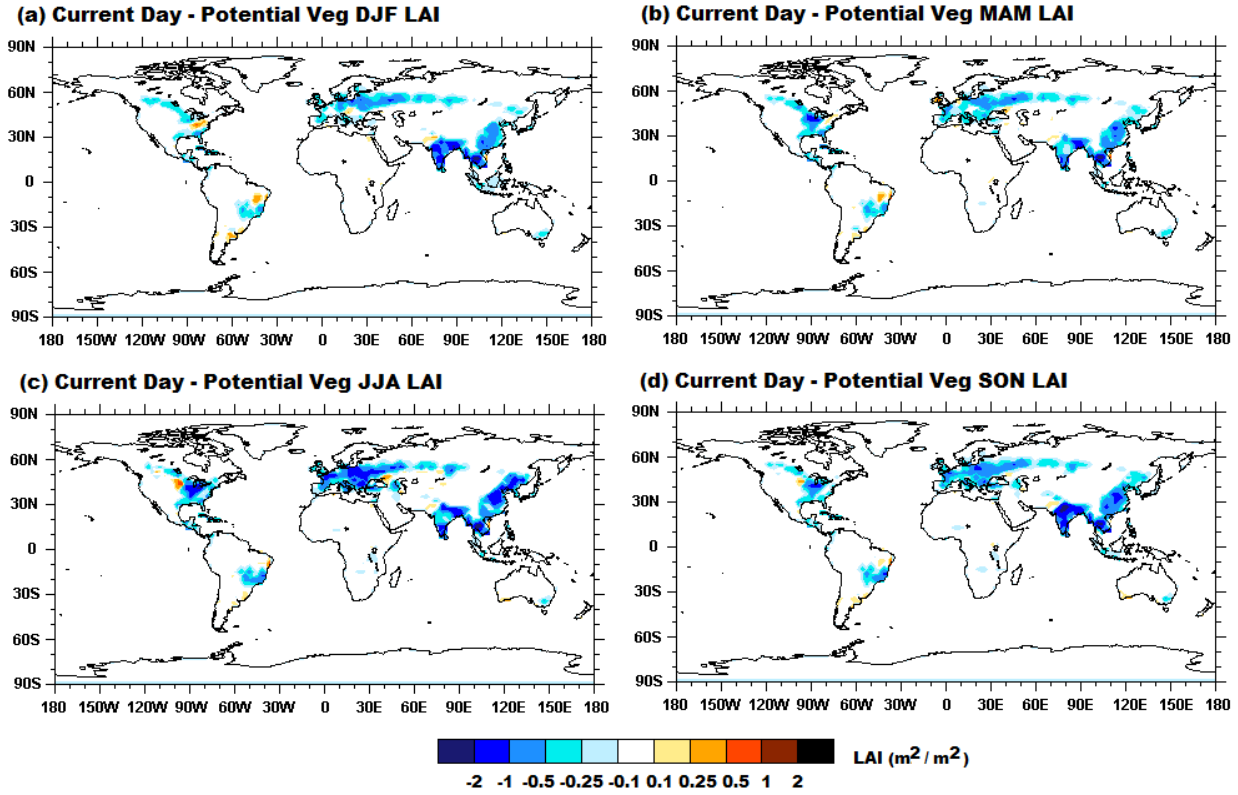

Figure 3. Land cover change in CLM Seasonal Leaf Area Index (LAI) between Current Day and Potential Vegetation Parameters.

4. Climate Impacts of Land Cover Change in CCSM with prescribed SSTs

4.1. Changes in Near Surface Air Temperature

The All Land and regional impacts of land cover change on near surface air temperature are tabulated in *Table 4* and mapped globally in *Figure 4*. The All Land analysis shows that CCSM with current day land surface parameters was 0.08^{O}C warmer for boreal summer (JJA) and 0.10^{O}C warmer for autumn (SON) than with the potential vegetation. In boreal winter (DJF) it was cooler by 0.01^{O}C however, resulting in annual average temperatures that were 0.04^{O}C warmer.

The maps in *Figure 4* show the higher temperatures in JJA and SON closely followed the land cover changes in the parameters. In DJF and MAM however, temperature changes show a divergence, with tropical and subtropical land cover changes resulting in warming and higher latitude northern land cover change resulting in cooling. The regional analysis also reflected this pattern with year round warming for India and Brazil, and summer warming and winter cooling for Europe, China and North America.

Table 4. Prescribed SST ensemble mean change in Average All Land and Regional land 2 meter air temperature (Degrees C) between Current Day and Potential Vegetation experiments.

Season	All Land	India	Europe	China	Brazil	North America
DJF	-0.01 w	+0.87 b	-0.32 b	-0.48 b	+0.24 b	-0.31 b
MAM	+0.01 w	+0.71 b	+0.04 w	+0.20 b	+0.24 b	+0.14 w
JJA	+0.08 b	+0.50 b	+0.36 b	+0.49 b	+0.22 b	+0.13 b
SON	+0.10 b	+0.86 b	+0.07 t	+0.13 w	+0.26 b	+0.12 w
Annual	+0.04 b	+0.74 b	+0.03 w	+0.08 n	+0.24 b	+0.02 n

** Statistical significance in differences between Current Day and Potential Vegetation experiments are shown as: n neither test has significance >= 0.95; t Student T-Test has significance >= 0.95; w Wilcoxon Signed Rank Test has significance >= 0.95; and b both tests have significance >= 0.95*

The Indian region had the largest annual and seasonal warming, with temperatures 0.74^{O} C higher as an annual average. The warming in India was largest in the winter (DJF) and late wet season (SON), with less warming in the late dry season (MAM) and early monsoon (JJA). The next largest warming was in Brazil were temperatures were 0.24^{O} C higher annually. The warming in Brazil was relatively consistent for all seasons, with the beginning of the rainy season (SON) having the largest warming and the winter dry season (JJA) having the smallest. Europe, China and North America all had substantially smaller annual warming than the tropical regions, as the summer (JJA), spring (MAM) and autumn (SON) warming were offset by the winter cooling (DJF).

4.2. Changes in Precipitation

The impacts of land cover change on precipitation are tabulated in *Table 5* and mapped in *Figure 4*. Over All Land the land cover change resulted in a marginal decrease in precipitation of 0.01 mm/day. The global maps and the regional analysis however show there were significant localized and seasonal changes in precipitation. China had the largest decrease in annual precipitation, with a reduction of 0.09 mm/day. The China region had decreases in precipitation for all seasons, with the largest decreases in summer (JJA), and the smallest decreases in winter (DJF).

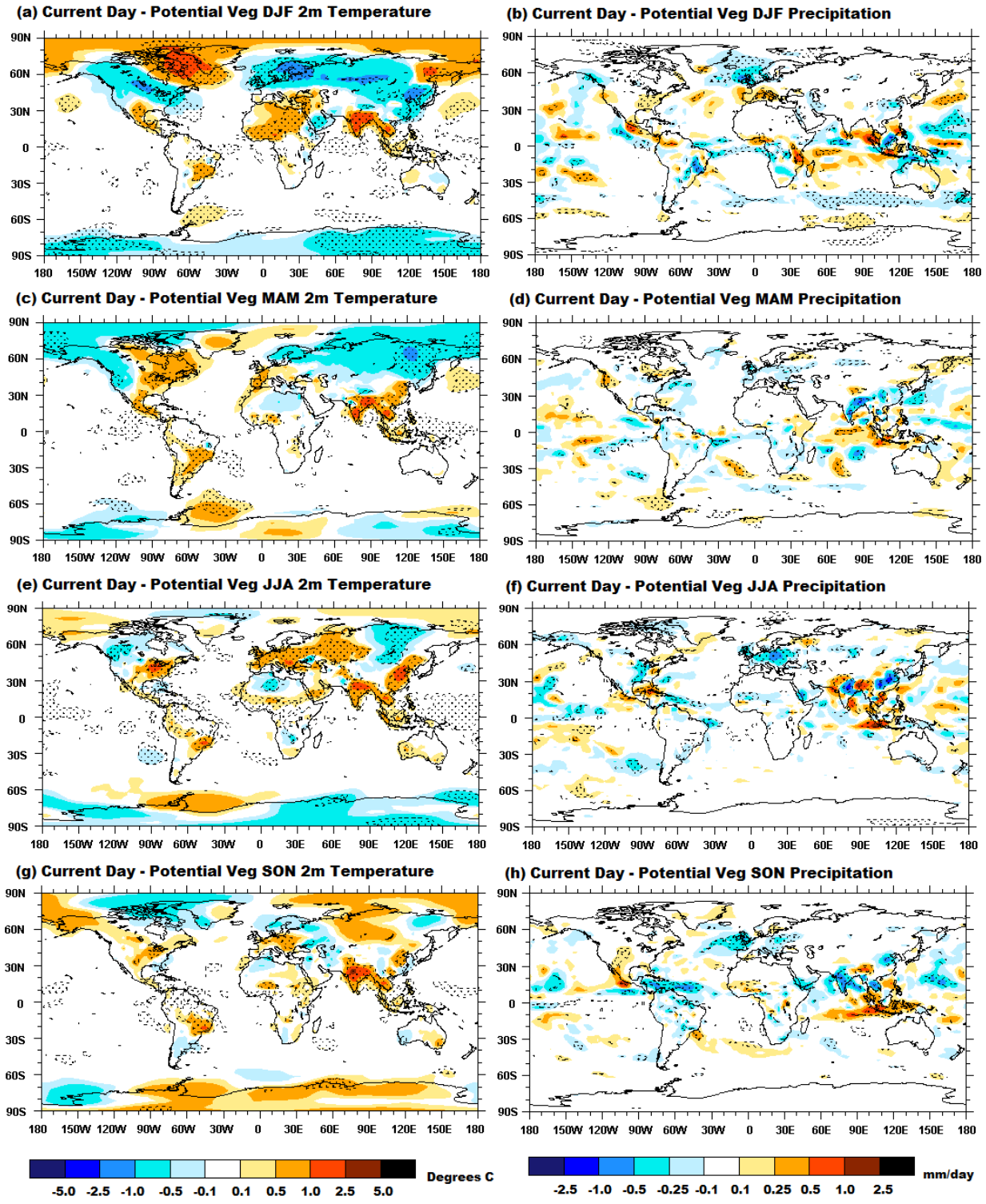

Figure 4. Prescribed SST Ensemble mean Climate Impacts of Land Cover Change between Current Day and Potential Vegetation experiments for: Reference Height Air Temperature (a, c, e and g); and Precipitation (b, d, f and g). Differences with statistical significance greater than 95% are stippled

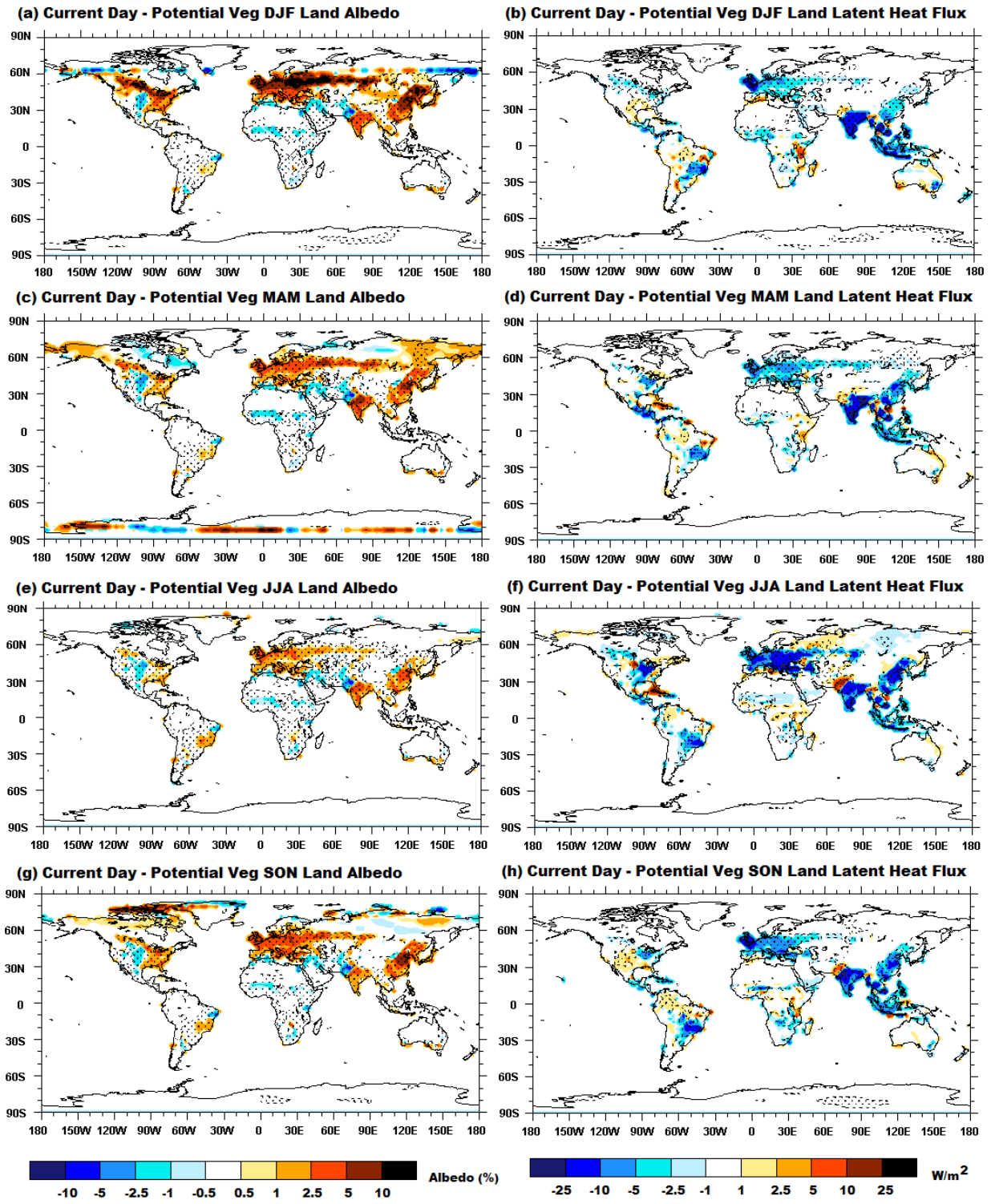

Figure 5. Prescribed SST Ensemble mean Climate Impacts of Land Cover Change between Current Day and Potential Vegetation experiments for: Land Broadband Albedo (a, c, e and g); and Land Latent Heat Flux (b, d, f and g). Differences with statistical significance greater than 95% are stippled

The next largest decrease in annual precipitation was in Europe with a decrease of 0.08 mm/day. In Europe decreases in summer (JJA), autumn (SON) and spring (MAM) precipitation, outweighed a relatively small increase in winter (DJF) precipitation. Brazil had the next largest decrease in annual precipitation, with a decrease of 0.07 mm/day. In Brazil there were decreases in precipitation for all seasons, with the largest decrease in the rainy season (DJF), and the smallest in the dry season (JJA).

Table 5. Prescribed SST ensemble mean change in Average All Land and Regional Precipitation (mm/day) between Current Day and Potential Vegetation experiments.

Season	All Land	India	Europe	China	Brazil	North America
DJF	0.00 n	+0.05 w	+0.02 w	-0.07 b	-0.12 t	+0.06 b
MAM	-0.01 n	-0.18 b	-0.07 t	-0.09 n	-0.07 n	+0.02 w
JJA	-0.02 t	+0.04 w	-0.16 b	-0.14 b	-0.04 t	-0.02 w
SON	-0.01 n	-0.14 b	-0.10 b	-0.08 w	-0.04 n	+0.05 w
Annual	-0.01 t	-0.06 w	-0.08 b	-0.09 b	-0.07 t	+0.02 b

** Statistical significance in differences between Current Day and Potential Vegetation experiments are shown as: n neither test has significance >= 0.95; t Student T-Test has significance >= 0.95; w Wilcoxon Signed Rank Test has significance >= 0.95; and b both tests have significance >= 0.95*

The changes in precipitation in India and North America were more complex than the other regions, with the seasonal changes combining to have a smaller reduction in annual precipitation for India, and a small increase in precipitation for North America. In India larger decreases in late dry season (MAM) and late monsoon season (SON) precipitation were partially offset by smaller increases in early monsoon (JJA) and winter (DJF) precipitation. In North America the increases in winter (DJF), autumn (SON), and spring (MAM) precipitation, outweighed the relatively small decrease in summer (JJA) precipitation.

4.3. Changes in Land Surface Albedo

The impacts of land cover change on broadband surface albedo are tabulated in *Table 6* and mapped in *Figure 5*. The All Land analysis shows the current day parameters resulted in surface albedo that was on annual average 0.4% higher (% of radiation reflected). The All Land increase in surface albedo was largest in boreal winter (DJF) with an increase of 0.68%, and smallest in summer (JJA) with an increase of 0.19%. The global mapping shows the increase in DJF albedo was largest at higher latitudes in the Northern Hemisphere, corresponding with areas where snow interacts with crops that were transformed from boreal and temperate forests. The mapping also shows there were some areas where albedo was lower with the current day parameters than with the potential vegetation parameters. These decreases typically corresponded with areas where grassland and shrubland were transformed to crops.

The regional analysis reflected the larger increase in DJF albedo in northern higher latitudes with Europe, China and North America all having their largest increases in DJF. Europe had the largest seasonal and annual increases in albedo, with DJF 5.05% higher, and the annual average albedo 2.87% higher. China had the next largest increases in albedo, with DJF 3.35% higher and the annual average 2.19% higher. India had the third largest increase in albedo, with annual albedo 1.39% higher. In India however, the seasonal increases were largest in the late dry season (MAM), where albedo was 1.92% higher.

North America had smaller increases in albedo than the other northern latitude regions, with DJF only 1.40% higher and the annual average albedo only 0.57% higher. The global mapping shows that in North America grassland conversion to crops in the mid-west resulted in lower albedo year round, and that

offset the higher albedo associated with the conversion of forests to crops and grassland in other parts of the region. Brazil had the lowest increase in albedo of all the regions, with an increase of only 0.19%. In Brazil the largest seasonal increase in albedo occurred in the dry season (JJA), as an increase of 0.40%.

Table 6. Prescribed SST ensemble mean change in Average All Land and Regional Land Surface Albedo (% radiation reflected) between Current Day and Potential Vegetation experiments.

Season	All Land	India	Europe	China	Brazil	North America
DJF	+0.68 b	+1.62 b	+5.05 b	+3.35 b	+0.03 b	+1.40 b
MAM	+0.37 b	+1.92 b	+2.24 b	+1.79 b	+0.17 b	+0.33 b
JJA	+0.19 b	+1.15 b	+1.47 b	+1.29 b	+0.40 b	+0.10 b
SON	+0.34 b	+0.85 b	+2.74 b	+2.30 b	+0.16 b	+0.43 b
Annual	+0.40 b	+1.39 b	+2.87 b	+2.19 b	+0.19 b	+0.57 b

** Statistical significance in differences between Current Day and Potential Vegetation experiments are shown as: n neither test has significance >= 0.95; t Student T-Test has significance >= 0.95; w Wilcoxon Signed Rank Test has significance >= 0.95; and b both tests have significance >= 0.95*

4.4. Changes in Land Latent Heat Flux

The impacts of land cover change on latent heat flux are tabulated in *Table 7* and mapped in *Figure 5*. Over All Land the current day parameters resulted in a reduction of annual average latent heat flux of 1.21 W/m^2, with the reduction largest in boreal summer (JJA) and smallest in spring (MAM). The global mapping shows the reduction in latent heat flux corresponded with areas of land cover change in terms of loss of trees and loss of LAI for all seasons (*Figures 2* and *3*). There are some areas however, where latent heat flux increased with the current day parameters. The Indus valley in Pakistan had a large increase in JJA latent heat flux, with smaller increases in other seasons. This was associated with current day densely vegetated cropping replacing sparsely vegetated shrublands in the potential vegetation. There also were small increases in latent heat flux in the American south-west, the northern Amazon, and central Africa.

Table 7. Prescribed SST ensemble mean change in Average All Land and Regional Land Latent Heat Flux (W/m^2) between Current Day and Potential Vegetation experiments.

Season	All Land	India	Europe	China	Brazil	North America
DJF	-1.16 b	-9.90 b	-3.23 b	-2.28 b	-2.22 b	-0.43 b
MAM	-1.13 b	-11.65 b	-3.60 b	-3.90 b	-1.97 b	-0.38 n
JJA	-1.40 b	-8.16 b	-8.28 b	-6.11 b	-3.33 b	-1.09 b
SON	-1.16 b	-8.65 b	-4.64 b	-4.23 b	-3.96 b	+0.01 w
Annual	-1.21 b	-9.59 b	-4.93 b	-4.13 b	-2.87 b	-0.48 b

** Statistical significance in differences between Current Day and Potential Vegetation experiments are shown as: n neither test has significance >= 0.95; t Student T-Test has significance >= 0.95; w Wilcoxon Signed Rank Test has significance >= 0.95; and b both tests have significance >= 0.95*

The regional analysis reflected the All Land analysis with all regions having decreased latent heat flux with the current day parameters. India with the greatest land cover change, tree loss and decrease in LAI, had the largest decrease in latent heat flux, with an annual average reduction of 9.59 W/m^2. The decrease in Indian latent heat flux was largest in the late dry season (MAM), and smallest in the early monsoon (JJA). Europe had the next largest decrease in latent heat flux, with an annual average reduction of 4.93

W/m^2. The decrease in European latent heat flux was largest in summer (JJA) and smallest in winter (DJF).

China had the third largest decrease in latent heat flux, with an annual average reduction of 4.13 W/m^2. In China the decrease in latent heat flux was largest in summer (JJA) and smallest in winter (DJF). Brazil had the second smallest decrease in latent heat flux, with an annual average reduction of 2.87 W/m^2. The Brazilian decrease in latent heat flux was largest in the dry season (JJA) and the early rainy season (SON), and smallest in the rest of the rainy season (DJF and MAM).

North America had the smallest decreases in latent heat flux, with an annual average reduction of only 0.48 W/m^2. The North American decrease in latent heat flux was largest in summer (JJA), smaller in winter (DJF) and spring (MAM), and an increase in autumn (SON). The difference in the latent heat flux changes in North America reflected the competing effects of grassland conversion to crops compared with the conversion of forests to crops and pasture.

4.5. Land Cover Forcing, Surface Energy Fluxes and Surface Hydrology

To further investigate the climate mechanisms that were changed with the changes in land cover, we analyzed the changes in temperature and precipitation against changes in the key forcing processes of albedo, cloud cover and LAI, and against changes in land surface energy fluxes and land surface hydrology. The mean monthly plots of these processes are shown in *Figure 6* for All Land, and the regions of India and Europe, and in *Figure 7* for the regions of China, Brazil, and North America.

The forcing changes for All Land (*Figure 6a*) show the current day parameters had year round lower LAI, and higher albedo, with a larger increase in albedo in boreal winter (DJF) than summer (JJA). The cloud cover changes however show considerable month to month variability in cloud response, with DJF and JJA both lower, and the other seasons mixed for the current day experiments. The All Land surface energy fluxes (*Figure 6b*) show the combined impact of the changes in albedo and cloud forcing, with the absorbed shortwave radiation lower for December through May, and higher for July and August. This shows the dominant forcing on shortwave radiation for most months was the higher albedo, but in July and August the lower cloud cover became dominant, allowing more incoming radiation to be absorbed by the land surface despite the higher albedo.

The biggest change in the All Land surface energy balance was the year round decrease in latent heat flux. This was offset by increases in outgoing longwave radiation and sensible heat flux, and a much smaller increase in ground heat flux. The decrease in latent heat flux, and increases in sensible and longwave fluxes were considerably larger than the changes in absorbed shortwave radiation. The changes in All Land surface hydrology (*Figure 6c*) show that the decrease in latent heat flux was primarily in response to reduced transpiration and canopy evaporation that resulted from the decrease in LAI and the changes in vegetation PFTs. These two decreases offset the increase in soil evaporation associated with a more open canopy and the lower evaporative demand from plants and canopy interception. The reduction in All Land evaporation and transpiration was realized through increased total runoff, and offset by the small decrease in precipitation.

In India (*Figure 6 d, e,* and *f*) the albedo impacts on shortwave radiation were only important for December through March, where shortwave radiation was reduced through the higher albedo. In other months cloud and albedo interactions resulted in mixed impacts on shortwave radiation. Again the biggest impact of the land cover change was the reduced latent heat flux, and the associated increases in sensible heat flux and outgoing longwave radiation. The surface hydrology changes show that the decrease in latent heat flux was smallest during the early monsoon (July – September) when the increase in soil evaporation was largest, and larger in other months when the soil evaporation had less influence.

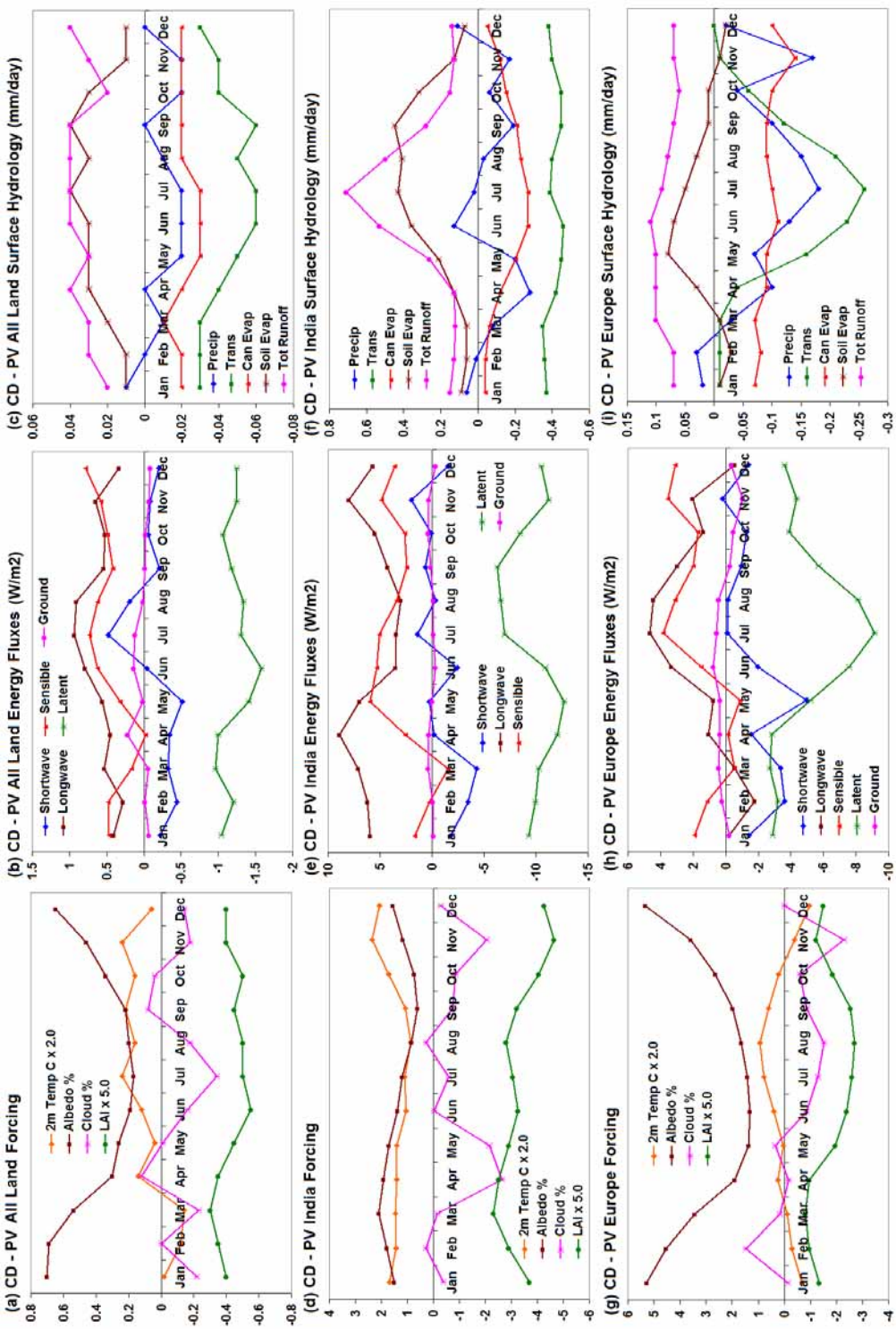

Figure 6. Prescribed SST Ensemble mean Climate Impacts of Land Cover Change between Current Day and Potential Vegetation experiments for the regions of All Land, India and Europe for: Climate Forcing (a, d, and g); Surface Energy Fluxes (b, e, and h); and Surface Hydrology (c, f, and i). All energy and moisture fluxes are out of the surface except Shortwave Radiation and Precipitation.

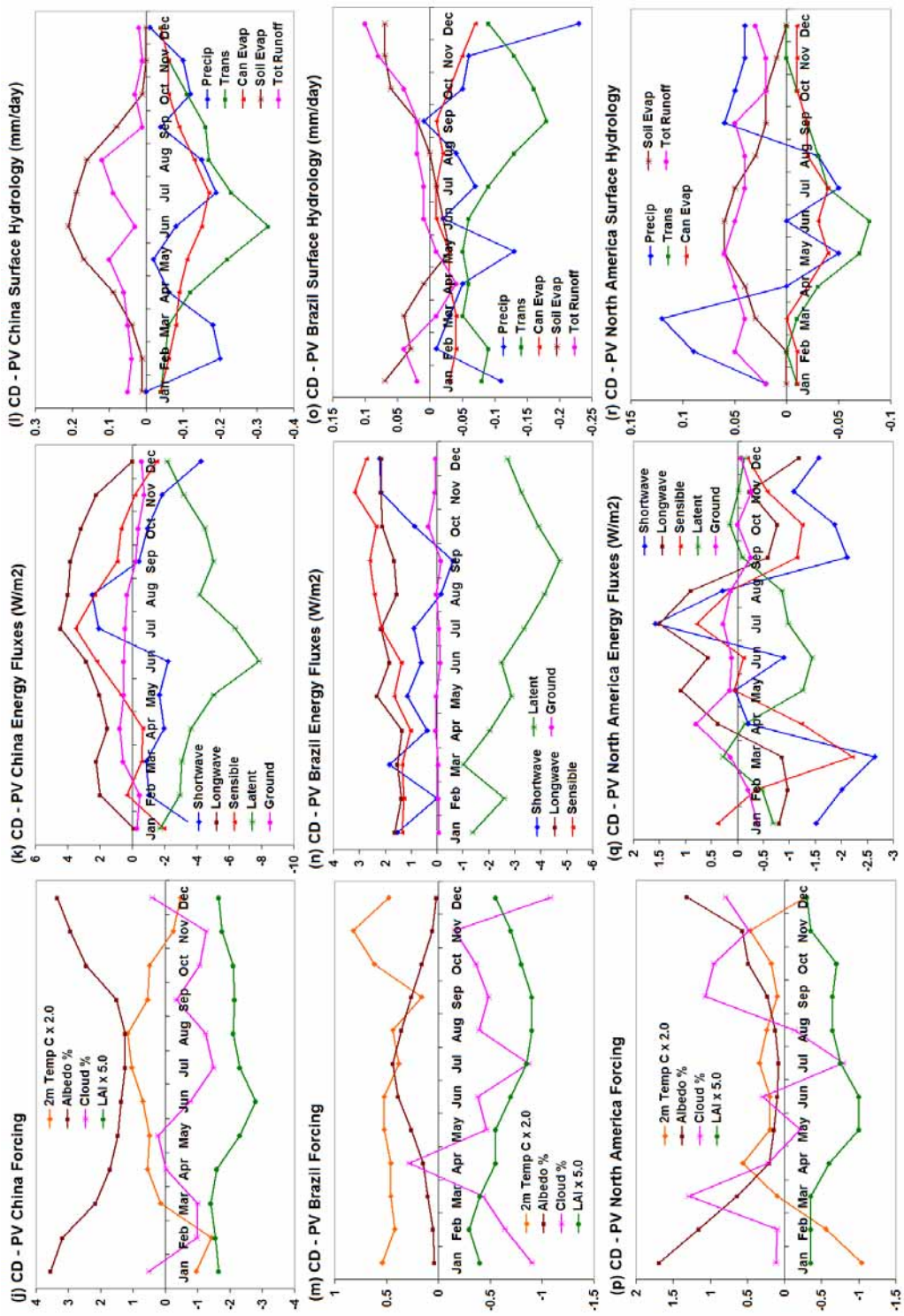

Figure 7. Same as Figure 6 except for the regions of China, Brazil and North America

In Europe (*Figure 6 g*, *h*, and *i*), the albedo forcing was largest in winter (DJF), and the LAI forcing was largest in summer (JJA). From December to June the higher albedo and cloud cover combined to reduce absorbed shortwave radiation, while in other months the impact of cloud cover offset the smaller increase in albedo resulting in little change to shortwave radiation. The seasonality of the LAI forcing was also evident on latent heat flux and transpiration, with the reduction in summer (JJA) transpiration and latent heat flux much larger than in other months. These two factors help explain the JJA warming and DJF cooling found in this region.

The forcing changes in China were very similar to Europe, with a similar impact on surface energy fluxes and surface hydrology. The main difference was in China the reduced JJA cloud resulted in increased absorbed shortwave radiation adding to the warming associated with reduced latent heat flux. The forcing changes in Brazil were very similar to India, but offset six months reflecting the Southern Hemisphere location. In Brazil however the reduced cloud dominated the higher albedo for most of the year with higher absorbed shortwave under current day parameters. Again the largest decrease in latent heat flux was in the dry season (July – October).

The North American region was different to the other regions in that the changes in latent heat flux were smaller than the changes in absorbed shortwave radiation. From September through April the higher albedo combined with higher cloud cover to reduce shortwave radiation. In July and August however the lower cloud cover resulted in higher shortwave radiation. The latent heat flux changes were not just different in magnitude to other regions, but in sign as well. In March and October the current day parameters had higher latent heat flux than the potential vegetation. This was a result of increased soil evaporation that exceeded decreases in transpiration and canopy evaporation for those months. The larger increase in soil evaporation was partly in response to the increase in September to March precipitation.

5. Climate Impacts of Land Cover Change in CCSM with coupled Ocean and Ice Models

5.1. Changes in Near Surface Air Temperature

The global and regional impacts of land cover change on near surface temperature with fully coupled ocean and ice models is tabulated in *Table 8* and mapped in *Figure 8*. The global analysis shows that overall the impact of land cover change in CCSM was warming of 0.02^{O} C annually. This was around a third of the warming found over All Land. The addition of the coupled ocean and ice models resulted in slightly higher annual warming over All Land compared to the experiments with prescribed SSTs and sea ice. The coupled experiments also changed the DJF cooling to a warming.

The global maps show that the tropical warming over India, the Amazon, and Africa found in the prescribed SST experiments was robust in the coupled experiments, as was the summer (JJA) and autumn (SON) warming over Europe, China and areas of North America. The maps also show that the high latitude Northern Hemisphere winter (DJF) cooling was less robust to feedbacks in ocean heat content, sea surface temperatures, and sea ice distributions, with the location of the cooling moving and some areas changing from cooling to warming.

The regional analysis reflected the robustness of the prescribed SST results. India again had the largest warming, with temperature annually warmer by 0.71^{O} C compared to 0.74^{O} C with the prescribed SSTs. The coupled models did change the seasonality of the warming, with the smallest warming in the late dry season (MAM) rather than in the early wet season (JJA). In Europe and China the coupled experiments had the same winter (DJF) cooling and summer (JJA) warming, however the magnitude of both of these were reduced compared to the prescribed SST experiments. In Brazil the warming was similar in both sets of experiments. In North America winter (DJF) cooling and summer (JJA) warming were both smaller

with the coupled models, but autumn (SON) warming was larger and spring (MAM) warming was changed to cooling reflecting a general lack of robustness for temperature changes over this region.

Table 8. Coupled Ocean and Ice Model change in Average Global and Regional 2 meter Air Temperature (Degrees C) between Current Day and Potential Vegetation experiments.

Season	Global	All Land	India	Europe	China	Brazil	N. America
DJF	+0.02 w	+0.06 w	+0.74 b	-0.14 w	-0.31 b	+0.25 b	-0.11 b
MAM	-0.01 n	-0.00 n	+0.40 b	-0.03 w	+0.05 w	+0.28 b	-0.04 w
JJA	+0.03 t	+0.09 b	+0.72 b	+0.32 b	+0.52 b	+0.17 b	+0.04 w
SON	+0.01 w	+0.06 t	+0.98 b	+0.21 b	+0.04 w	+0.21 b	+0.21 b
Annual	+0.02 w	+0.05 w	+0.71 b	+0.09 w	+0.07 n	+0.23 b	+0.02 w

** Statistical significance in differences between Current Day and Potential Vegetation experiments are shown as: n neither test has significance >= 0.95; t Student T-Test has significance >= 0.95; w Wilcoxon Signed Rank Test has significance >= 0.95; and b both tests have significance >= 0.95*

5.2. Changes in Precipitation

The global and regional impacts of land cover change on precipitation in CCSM with coupled ocean and ice models are tabulated in *Table 9* and mapped in *Figure 8*. The global analysis shows the impact of the land cover change was a reduction in global precipitation of 0.01 mm/day. This was the same as the reduction in precipitation over All Land, and the same as the reduction in precipitation found in the prescribed SST experiments over All Land. The global maps show that the changes in precipitation over the oceans were much larger with the coupled models than with the prescribed SSTs (*Figure 4*). The maps also show there were similar changes in precipitation over many areas of land cover change in both sets of experiments.

Table 9. Coupled Ocean and Ice Model change in Average Global and Regional Precipitation (mm/day) between Current Day and Potential Vegetation experiments.

Season	Global	All Land	India	Europe	China	Brazil	N. America
DJF	-0.00 n	-0.01 n	-0.05 b	-0.08 b	-0.17 b	-0.02 w	-0.04 w
MAM	-0.02 b	-0.01 t	-0.29 b	-0.05 w	-0.20 t	-0.10 w	-0.01 n
JJA	-0.02 b	-0.03 t	-0.35 b	-0.19 b	-0.12 t	-0.00 w	-0.04 n
SON	-0.01 b	-0.02 n	-0.20 b	-0.08 b	-0.03 w	-0.09 w	+0.01 w
Annual	-0.01 b	-0.01 t	-0.22 b	-0.09 b	-0.13 b	-0.04 w	-0.02 n

** Statistical significance in differences between Current Day and Potential Vegetation experiments are shown as: n neither test has significance >= 0.95; t Student T-Test has significance >= 0.95; w Wilcoxon Signed Rank Test has significance >= 0.95; and b both tests have significance >= 0.95*

The regional analysis highlighted the similarities and differences in precipitation change between the experiments with coupled models compared to with prescribed SSTs and sea ice. With the coupled models the region with the largest decrease in annual precipitation changed from China to India. The Indian region had three times the reduction in annual precipitation with the coupled models, being 0.22 mm/day lower than the potential vegetation. There also were changes in the seasonality with India having lower precipitation for all seasons, rather than redistributing the precipitation between seasons.

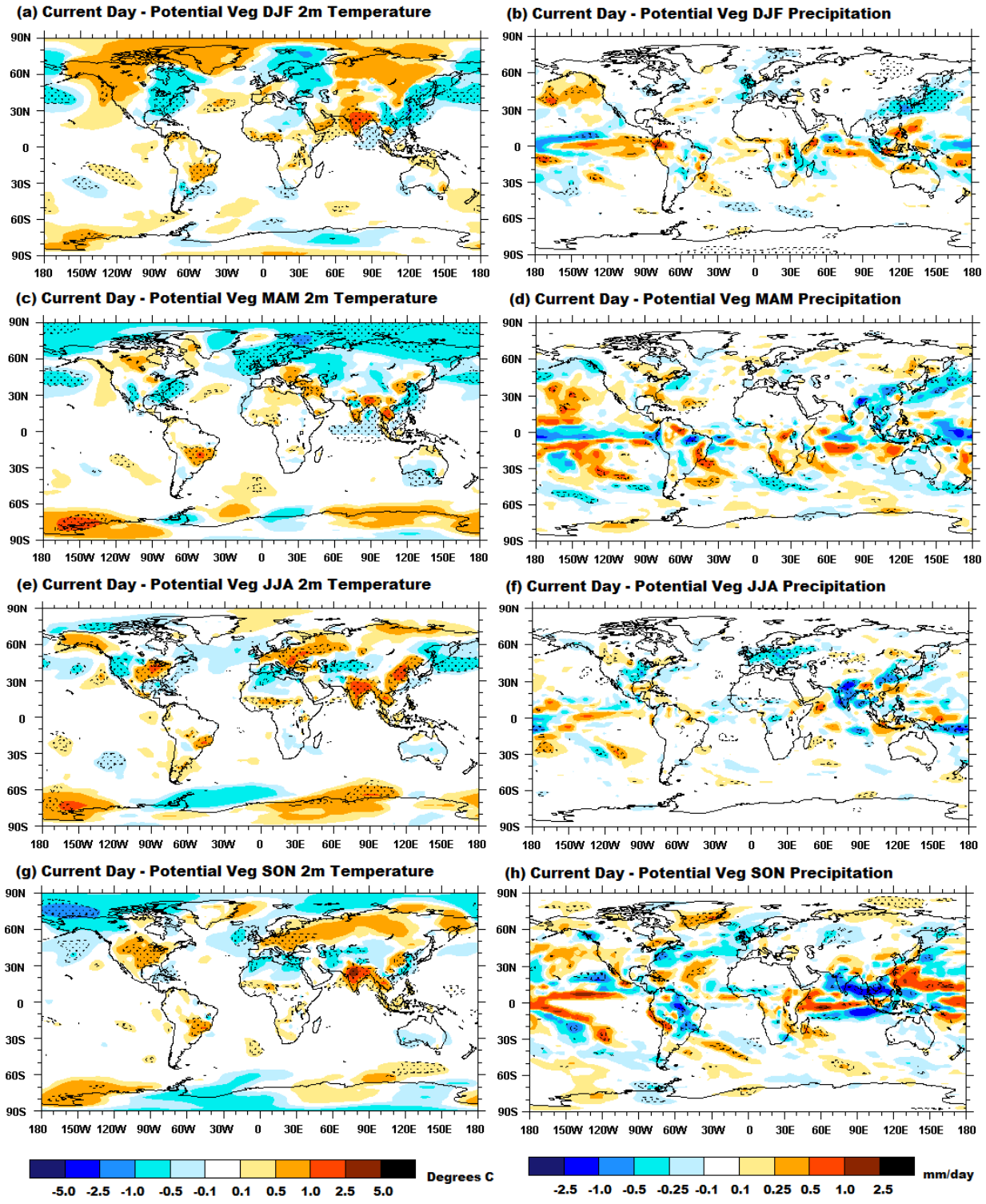

Figure 8. Coupled Ocean and Ice mean Climate Impacts of Land Cover Change between Current Day and Potential Vegetation experiments for: Reference Height Air Temperature (a, c, e and g); and Precipitation (b, d, f and g). Differences with statistical significance greater than 95% are stippled

With the coupled models, China had the next largest reduction in precipitation, with annual precipitation reduced by 0.13 mm/day. This was 0.05 mm/day larger than the decrease with prescribed SSTs. Winter (DJF) and spring (MAM) decreases in precipitation were larger, however summer (JJA) and autumn (SON) decreases were smaller. The decrease in European precipitation was similar with the coupled models at 0.09 mm/day, however the seasonality of change was different. The summer (JJA) reduction was larger, the winter (DJF) increase in precipitation changed to a decrease, and the spring (MAM) and autumn (SON) decreases were smaller.

In Brazil the coupled model experiments had a smaller decrease in annual precipitation at 0.04 mm/day. The seasonality of the decrease also changed with smaller decreases in the rainy season (DJF) and the dry season (JJA), and bigger increases in the other seasons. In North America the coupled model experiments changed from an increase in annual precipitation to a decrease of 0.02 mm/day. This change was predominantly in the winter (DJF), but was evident in all seasons.

5.3. Changes in Annual Forcing, Surface Energy Fluxes, and Top of Atmosphere Radiative Fluxes

The annual average changes in radiative forcing and energy fluxes are tabulated in *Table 10*. These annual changes provide insight into the global and regional forcing and climate response in the fully coupled CCSM to land cover change. At a global level the increase in albedo is a quarter of the value found for All Land, reflecting the contribution of land to total global surface area. The All Land and regional increases in albedo are all consistent with the increases found in the prescribed SST experiments, demonstrating the robustness of the albedo response to land cover change.

Table 10. Coupled Ocean and Ice Model change in average Global and Regional Annual Surface Albedo (% of radiation reflected), Cloud Cover (%), surface energy fluxes (W/m^2), and top of the atmosphere energy fluxes (W/m^2) between Current Day and Potential Vegetation experiments. All energy fluxes are out of the surface or top of the atmosphere except Shortwave Radiation.

Season	Global	All Land	India	Europe	China	Brazil	N. America
Albedo	+0.09 b	+0.36 b	+1.46 b	+2.65 b	+2.07 b	+0.19 b	+0.39 b
Cloud	-0.07 b	-0.13 w	-1.48 b	+0.68 w	-1.23 b	-0.72 w	-0.31 w
Shortwave	+0.11 b	-0.05 w	+0.66 b	-1.71 b	-0.85 b	+1.06 b	-0.18 w
Longwave	+0.19 b	+0.68 b	+7.31 b	+1.59 b	+2.87 b	+1.68 b	+0.72 b
Latent	-0.27 b	-1.43 b	-12.25 b	-4.94 b	-5.00 b	-2.49 b	-1.18 b
Sensible	+0.17 b	+0.70 b	+5.55 b	+1.61 b	+1.27 b	+1.86 b	+0.29 b
Shortw TOA	+0.10 b	+0.05 w	+0.73 b	-1.11 b	-0.41 w	+0.95 b	-0.14 w
Longw TOA	+0.06 b	+0.07 w	+2.31 b	+0.20 w	+0.81 b	+0.48 w	+0.15 w

** Statistical significance in differences between Current Day and Potential Vegetation experiments are shown as: n neither test has significance >= 0.95; t Student T-Test has significance >= 0.95; w Wilcoxon Signed Rank Test has significance >= 0.95; and b both tests have significance >= 0.95.*

The global decrease in cloud cover however, was more than half of the All Land value, reflecting decreases in cloud over oceans and sea ice in the current day experiment. This had impacts on radiation budgets beyond the land surface and areas of land cover change. The All Land and regional changes in cloud cover were all decreases except for Europe which had an increase. The lower global and regional cloud cover corresponded with the reduced global and regional latent heat flux indicating a possible cloud response to the reduced evapo-transpiration with the current day parameters.

The changes in global and All Land absorbed shortwave radiation demonstrate the interactions between the increased albedo and reduced cloud cover. At a global level the absorbed shortwave radiation was higher with the current day parameters, despite higher global surface albedo. At this level, the reduced cloud cover was more important than the higher albedo. For All Land however, this relationship was reversed, with the shortwave radiation lower despite reduced cloud cover. This is an important response as the IPCC 4th assessment report [*Forster, et al.*, 2007] uses the albedo forcing on land to suggest the radiative impact of land cover change since 1750 is global cooling, however this does not take into account other possible radiative forcing such as the indirect forcing through changes in cloud cover.

The regional changes in absorbed shortwave radiation also reflect the competing effects of surface albedo and cloud cover. In India and Brazil the reduced cloud cover dominates the higher albedo to result in increased shortwave radiation. In China and North America the higher albedo dominates the reduced cloud cover resulting in lower shortwave radiation. And in Europe the higher albedo combines with higher cloud cover to reduce shortwave radiation even further.

As previously shown, latent heat flux was lower globally, over All Land, and in each of the regions. The global decrease in latent heat flux is a sixth of the All Land decrease, suggesting that increases in latent heat flux over the oceans partly compensated for the decrease in land latent heat flux. The decrease in latent heat flux is balanced by increased sensible heat flux and longwave radiation out of the surface globally, over All Land, and in all regions. The size of the decrease in latent heat flux corresponds directly with the size of the increases in sensible heat flux and longwave radiation out. This is an important relationship as it shows the upward surface energy flux changes associated with land cover change were robust and independent of the region investigated.

Radiatively at the top of the atmosphere the global increase in absorbed shortwave radiation was larger than the increase in outgoing longwave radiation, resulting in radiative warming of 0.04 W/m^2. Over All Land however, the increase in outgoing longwave radiation was greater than the increase in absorbed shortwave radiation resulting in a net radiative cooling of 0.02 W/m^2. All regions except Brazil had net radiative cooling at the top of the atmosphere as well. India had the largest cooling at 1.58 W/m^2, with Europe cooling at 1.31 W/m^2, China cooling at 1.22 W/m^2, and North America cooling at 0.29 W/m^2. The radiative warming over Brazil was relative small at 0.47 W/m^2.

6. Discussion and Conclusion

6.1. Describing Land Cover Change in CLM

The new methods for generating potential vegetation parameters for CLM allowed us to specify land cover change on the PFT level in CLM as suggested by [*Oleson, et al.*, 2004], while capturing the location and nature of land use change described by [*Ramankutty and Foley*, 1999]. Globally the land cover change between current day and potential vegetation CLM parameters replaced natural tree, shrub and grass PFTs with land use, principally cropping, resulting in substantially lower LAI and higher albedo for the current day.

The differences between the current day and potential vegetation parameters reflected the distinct regional nature of land cover change in terms of biomes and PFTs. India had the largest transformation to crops, followed by Europe and China. In these regions forests were predominantly replaced with crops, with the creation of pasture a secondary process. North America had the second smallest transformation to crops, and involved the widespread conversion of grassland to crops. This combined with smaller conversions of forests, resulting in losses of grass PFTs at similar levels to losses of needleleaf and broadleaf trees. This had impacts on the size of the albedo and LAI changes compared to other regions. Brazil had the smallest

transformation to crops, with a larger increase in grass PFTs. This reflected the widespread conversion of savanna and forest to pasture that was a major component of the land cover change in this region.

To assess the biome level differences in PFT contribution, broadband surface albedo, and LAI, the current day MODIS satellite derived data has been analyzed globally against the current day biome mapping at the 0.05 degree resolution of the raw data. The results of this analysis are tabulated as global averages in *Table 11*. From a PFT perspective there is good correspondence between the current day biomes derived from the AVHRR Global Land Cover Characterization (GLCC) of [*Loveland, et al.*, 2000], and their global average MODIS derived PFT composition from [*Lawrence and Chase*, 2007].

Table 11. Average global current day MODIS satellite derived: Plant Functional Types (PFTs) (% composition of first four PFTs); Grid cell average Leaf Area Index (LAI); and Broadband Surface Albedo (Albedo) (%) for the Current Day Biome distributions of [Ramankutty and Foley, 1999]. LAI and Albedo values are seasonal averages for Boreal Winter (DJF) and Summer (JJA).*

Biome	PFT1 (%)	PFT2 (%)	PFT3 (%)	PFT4 (%)	LAI		Albedo	
					DJF	JJA	DJF	JJA
Trop Evg For	BET (65)	BDT (15)	C (7)	GC4 (6)	3.6	3.9	12.8	12.7
Trop Dec For	BDT (22)	GC4 (20)	GC3 (20)	BET (10)	2.2	2.0	13.1	12.8
Temp Brd Evg	BEM (34)	GC3 (16)	NEM (15)	BDM (13)	2.3	2.0	11.9	12.0
Temp Ndl Evg	NEM (33)	NEB (22)	BDM (11)	C (11)	1.0	3.2	22.5	12.1
Temp Dec For	BDM (35)	C (20)	NEM (17)	GC3 (17)	0.9	3.4	19.4	14.5
Borl Evg For	NEB (67)	SDB (12)	GA3 (10)	BDB (4)	0.2	2.9	35.7	10.5
Borl Dec For	NDB (39)	NEB (25)	SDB (15)	GA3 (13)	0.1	3.3	39.3	11.7
Mixed Forest	SDB (28)	NEB (26)	GA3 (9)	B (7)	0.4	2.7	37.5	12.6
Savanna	GC4 (33)	GC3 (15)	BDT (12)	C (10)	1.2	1.5	17.0	14.8
Grassland	B (35)	GC3 (20)	C (10)	SDM (8)	0.4	0.7	31.8	17.3
Dense Shrub	B (31)	SDM (25)	GC4 (10)	GC3 (10)	0.7	0.8	17.0	17.0
Open Shrub	B (66)	SDM (17)	GC3 (6)	C (5)	0.2	0.3	25.7	21.7
Tundra	B (47)	SDB (32)	GA3 (15)	NEB (3)	0.1	0.8	47.0	17.7
Desert	B (97)	SDM (1)	GC3 (1)	GC4 (1)	0.0	0.0	33.9	32.2
Polar / Ice	-	-	-	-	0.0	0.0	75.0	69.3
Landuse	C (36)	GC3 (21)	GC4 (12)	B (7)	0.9	1.5	23.7	15.4
Wetland	-	-	-	-	1.4	1.9	17.5	7.4

** Plant Functional Types are: B, bare; NEM, needleleaf evergreen temperate tree; NEB, needleleaf evergreen boreal tree; NDB, needleleaf deciduous boreal tree; BET, broadleaf evergreen tropical tree; BEM, broadleaf evergreen temperate tree; BDT, broadleaf deciduous tropical tree; BDM, broadleaf deciduous temperature tree; BDB, broadleaf deciduous boreal tree; SEM, evergreen temperate shrub; SDM, deciduous temperate shrub; SDB, deciduous boreal shrub; GA3, c3 grass arctic; GC3, c3 grass non-arctic; GC4, c4 grass; and C, crop.*

The forest biomes are predominantly composed of trees of the correct leaf type and phenology. Savannas, grasslands, shrublands, and landuse also have consistent composition with their respective PFTs. There is some inconsistency with large crop contributions in temperate needleleaf and deciduous forests, and in savannas and grasslands. This inconsistency comes from differences in the fractional crop mapping of [*Ramankutty and Foley*, 1999] compared with the categorical GLCC land use class mapping. This issue

was dealt with in the parameter extrapolation process through secondary filtering that ensured all crops were excluded from the potential vegetation parameters.

The current day MODIS LAI mapping from [*Myneni, et al.*, 2002] is consistent with the biome mapping, with forest biomes having higher LAI than savannas, and with lower LAI values for grasslands, shrublands, tundra, and deserts. The LAI values for land use are higher than grasslands and shrublands, but considerably lower than forests. While the biome LAI values are global averages, the differences between the temperate deciduous forest, temperate needleleaf forest and land use biomes are consistent with the field observed differences in hardwood forest, pine forest and pasture LAI found at the Duke Forest in the southeastern United States by [*Juang, et al.*, 2007]. The raw MODIS LAI does have very low values for boreal evergreen forests in the winter (DJF), which is primarily a result of snow masking in the satellite data. In both sets of CLM land surface parameters these low satellite values are corrected through phenology rules as described in [*Lawrence and Chase*, 2007].

The current day MODIS albedo mapping from [*Schaaf, et al.*, 2002] is also consistent with the biome mapping, with forests having lower albedo than savannas, with increasingly higher albedo values found in grasslands, shrublands, tundra and deserts. The land use biome has higher albedo than forests, but lower albedo than grasslands, shrublands, tundra and deserts. The northern winter snow impact on albedo is highly evident for temperate and boreal forests, and for grasslands, land use and tundra, with DJF albedo considerably higher than JJA. The albedo of evergreen tropical forests is very close to the directly observed Amazon forest albedo (12.7% compared to 13.0%) reported by [*von Randow, et al.*, 2004] from the Large Scale Biosphere-Atmosphere Experiment in Amazonia (LBA) study.

The seasonal albedo values of the temperate deciduous forest, temperate needle forest, and land use also are very close to the observed values found at the Duke Forest by [*Juang, et al.*, 2007]. Additional field and satellite validation by [*Liang, et al.*, 2002] further demonstrates that the MODIS albedo data captures the surface shortwave radiation properties of a diverse range of land cover and soil types with high reliability. This provides an additional reference point as the differences in the current day MODIS albedo are reproduced in the land surface albedo changes of the CCSM land cover change experiments, even in areas with large snow interactions. Interestingly the JJA biome albedo values also are in good agreement with the snow free biome albedo values prescribed by [*Findell, et al.*, 2007].

Despite the consistency with previous work and the correspondence between changes in biomes and changes in land surface parameters, the spatial extent of land cover change in the experiments is highly conservative as the [*Ramankutty and Foley*, 1999] study is restricted to changes in land cover classes that represent human land use. This restricts land cover change to areas where human activity has transformed natural biomes to completely human landscapes. By only capturing landscape transformation the land cover change from human disturbance of natural biomes through forestry, grazing of natural biomes, and other activities are not included. This limitation is evident in areas such as Australia, where studies by [*Lawrence*, 2004] and [*McAlpine, et al.*, 2007] used local and national historic vegetation mapping, and found over three times the land cover change in LAI compared to this global study. This indicates that the spatial extent of land cover change may be substantially larger than captured in our experiments.

6.2. Climate Impacts of Land Cover Change in CCSM

The direct bio-geophysical climate impacts of land cover change in CCSM were the year round warming of the near surface atmosphere in tropical and subtropical regions, and the winter cooling and summer warming in higher northern latitudes. The tropical and summer warming was robust, with statistically significant results in both the prescribed SST experiments and the fully coupled experiments. The high latitude winter cooling was only significant with prescribed SSTs however. With the coupled ocean and sea ice models these cooling patterns and their statistical strength are both lost.

The experiments also show that changes in surface albedo and energy fluxes out of the surface were robust in both the prescribed SST and fully coupled model experiments. The surface hydrology and surface flux analysis shows that the warming was predominantly in response to reduced evapo-transpiration and therefore latent heat flux in the current day experiment, with radiative forcing playing a secondary role. The idea that replacing forests with grass and crop lands results in regional warming through reduced evapo-transpiration is not new. [*Baumgartner*, 1984] provides a detailed review from the early 1980s illustrating the competing influences of albedo and evapo-transpiration in a range of forests, identifying the warming impacts of deforestation.

The regional warming from tropical and subtropical deforestation has been supported by a range of studies by [*Lean and Warrilow*, 1989], [*Shulka, et al.*, 1990], [*Dickinson and Kennedy*, 1992], [*Polcher and Laval*, 1994], and [*Zhang, et al.*, 1995]. More recently these relationships have been further supported by studies and reviews by [*Feddema, et al.*, 2005], [*Chase, et al.*, 1996], [*Pielke*, 2001], [*Niyogi, et al.*, 2002], [*Findell, et al.*, 2007] and [*Bonan*, 2008]. Field observations at the Duke Forest by [*Juang, et al.*, 2007] also support the warming effects of deforestation for both mid-latitude hardwood broadleaf forests and pine forests. Compared to adjacent forests, pastures were warmer by 2.9^{O} C and 2.1^{O} C respectively, due to lower evapo-transpiration and reduced surface roughness. This dominated smaller cooling from higher albedo of 0.7^{O} C and 0.9^{O} C.

Also supporting the regional warming from deforestation, [*Lee, et al.*, 2005] found that deep rooted trees can redistribute deep soil moisture through the soil profile allowing them additional increases in transpiration in the dry season compared to shallow rooted grasses. In a similar manner, [*Leuning, et al.*, 2005] found that deep rooted *Eucalyptus* trees were able to reach soil moisture through the Australian drought of 2003 that was not available to grasses. In the LBA study, [*von Randow, et al.*, 2004] found that forests had 20% higher evapo-transpiration and 45% lower sensible heat flux in the wet season than nearby pastures, and 41% higher evapo-transpiration and 28% lower sensible heat flux in the dry season. The study also found that the trees were able to access soil water from deep in the soil profile while the pasture vegetation could only access water from the upper soil layers.

[*Giambelluca, et al.*, 2000] found the higher transpiration and latent heat flux of deep rooted trees also was evident in field observations of regenerating forests in the eastern Amazon and in northern Thailand. In both regions their observations found that the evaporative fraction of the surface energy budget and the latent heat fluxes increased with regeneration age of the forest from time of disturbance. Using simultaneous atmospheric soundings and satellite cloud observations, [*Wang, et al.*, 2009] found that forested areas in the Rondonian Amazon had higher humidity levels in the boundary layer and preferentially resulted in deep convection, compared to nearby pastures.

The role of surface hydrology found in European summer time warming also has been demonstrated by [*Fischer, et al.*, 2007], who found that dry soil conditions and soil moisture dynamics were key components leading to the record breaking European heat wave of 2003. In all of these field observations and modeling studies the surface hydrology is the dominating forcing from the land surface, with tropical and mid-latitude deforestation resulting in near surface warming through decreased evapo-transpiration that outweighs cooling through higher albedo.

Looking at other climate impacts of land cover change in the CCSM experiments shows there were robust changes in regional precipitation and on monsoon systems as well. The current day decreases in European and Brazilian precipitation were consistent for both the prescribed SST and fully coupled experiments. The decrease in Indian and Chinese precipitation was evident for both sets of experiments, however the coupled models substantially increased the size of the decrease in both of these regions. The impact of changes in surface fluxes on the Indian and Asian monsoons was consistent with other recent studies by

[*Lee, et al.*, 2009], [*Lobell, et al.*, 2006] and [*Douglas, et al.*, 2006], where lower latent heat flux over India and Asia results in decreased precipitation, warmer near surface temperatures, and altered monsoon circulation.

The role of clouds in the surface radiation budget also was highlighted, with the lower cloud cover associated with the reduced evapo-transpiration having a larger impact than albedo globally, which resulted in increased global shortwave radiation absorption. Despite these changes in global shortwave radiation and in surface energy fluxes, the net global impact of land cover change on near surface temperatures in CCSM was a minimal increase of 0.02^{O} C. This demonstrated that at a global level land cover change did not have a strong warming or cooling influence in CCSM, which was in agreement with the global findings of [*Findell, et al.*, 2009]. This was true of global precipitation as well.

6.3. Implications and Conclusions

Given that the decreases in evapo-transpiration and the regional warming found in the CCSM land cover change experiments were robust and supported by a wide range of field studies, satellite products, and regional and global climate modeling studies, understanding the mixed surface flux changes and climate forcing found in the LUCID study of [*Pitman, et al.*, 2009] is a priority to resolving uncertainties in simulating the climate impacts of global land cover change in GCMs. In the LUCID study only half of the modeling experiments had decreased latent heat flux associated with deforestation, while the other half had increased latent heat flux. What is evident from the CCSM experiments is that realistically simulating land surface forcing in a land cover change experiment requires the land surface model be able to reproduce the surface forcing found in field and satellite studies. From the LUCID experiments we can see that this is not the case for many of the current GCMs used in climate impacts of land cover change studies.

The robust decreases in evapo-transpiration and regional warming found in the CCSM experiments, and in the supporting field observations and modeling studies, have implications for future land use and the regional impacts of climate change under enhanced atmospheric greenhouse gas concentrations. As the land surface and the hydrological cycle continue to be modified through deforestation, urbanization, agricultural development, further reductions in evapo-transpiration may substantially enhance regional warming on top of projected global warming. This specifically has implications for widespread landscape conversion to agriculture for bio-fuel production. Conversely, the dominance of surface hydrology over albedo may be beneficial for carbon sequestration projects such as re-forestation, as the increased evapo-transpiration may be a cooling influence even in higher latitude forests, offsetting any potential global warming from lower albedo as suggested by [*Bala, et al.*, 2007], and [*Betts*, 2000].

Acknowledgements

The use of the computing time for the model experiments was supplied through a grant from the National Center for Atmospheric Research, Community Climate System Model (CCSM) Land Working Group, which is sponsored by the National Science Foundation. Funding for this research also was supported by National Science Foundation grants ATM 0639838, ATM0001476 and ATM0437538. MODIS land surface products were provided by the MODIS Land Science Team. Historical cropping and potential vegetation data were provided by the Center for Sustainability and the Global Environment, University of Wisconsin.

References

Bala, G., et al. (2007), Combined climate and carbon-cycle effects of large-scale deforestation, *Proceedings of the National Academy of Sciences*, *104*, 6550-6555.

Baumgartner, A. (1984), Effects of Deforestation and Afforestation on Climate, *GeoJournal*, *8*, 283-288.
Betts, R. A. (2000), Offset of the potential carbon sink from boreal forestation by decreases in surface albedo, *Nature*, *408*, 187-190.
Betts, R. A., et al. (2001), Biogeophysical effects of land use on climate: Model simulations of radiative forcing and large-scale temperature change, *Agricultural and Forest Meteorology*, *142*, 216-233.
Bonan, G. B. (2008), Forests and Climate Change: Forcings, Feedbacks, and the Climate Benefits of Forests, *Science*, *320*, doi:10.1126/science.1155121.
Brovkin, V., et al. (1999), Modeling climate response to historical land cover change, *Global Ecology and Biogeography*, *8*, 509-517.
Chase, T. N., et al. (1996), Sensitivity of a general circulation model to global changes in leaf area index, *Journal of Geophysical Research*, *101*, 7393-7408.
Dickinson, R. E., and P. Kennedy (1992), Impacts on regional climate of Amazon deforestation, *Geophysical Research Letters*, *19*, 1947-1950.
Douglas, E. M., et al. (2006), Changes in moisture and energy fluxes due to agricultural land use and irrigation in the Indian monsoon belt, *Geophysical Research Letters*, *33*, doi:10.1029/2006GL026550.
Feddema, J. J., et al. (2005), The Importance of Land-Cover Change in Simulating Future Climates, *Science*, *310*, 1674 - 1678.
Findell, K. L., et al. (2009), Regional and Global Impacts of Land Cover Change and Sea Surface Temperature Anomalies, *Journal of Climate*, *22*, 3248-3269.
Findell, K. L., et al. (2007), Modeled Impact of Anthropogenic Land Cover Change on Climate, *Journal of Climate*, *20*, DOI: 10.1175/JCLI4185.1171.
Fischer, E. M., et al. (2007), Soil Moisture-Atmosphere Interactions during the 2003 European Summer Heat Wave, *Journal of Climate*, *20*, 5081-5099.
Forster, P., et al. (2007), Changes in Atmospheric Constituents and in Radiative Forcing., in *Climate Change 2007:*
The Physical Science Basis. Contribution of Working Group I to the Fourth Assessment Report of the Intergovernmental Panel on Climate
Change [Solomon, S., D. Qin, M. Manning, Z. Chen, M. Marquis, K.B. Averyt, M.Tignor and H.L. Miller (eds.)], edited, Cambridge University Press, Cambridge, United Kingdom and New York, NY, USA.
Friedl, M., et al. (2002), Global land cover mapping from MODIS: algorithms and early results, *Remote Sensing of Environment*, *83*, 287-302.
Giambelluca, T. W., et al. (2000), Latent and Sensible Energy Flux Over Deforested Land Surfaces in the Eastern Amazon and Northern Thailand, *Singapore Journal of Tropical Geography*, *21*, 107-130.
Haxeltine, A., and I. C. Prentice (1996), BIOME3: An equilibrium terrestrial biosphere model based on ecophysical constraints, resource availability, and competition among plant functional types, *Global Biogeochemical Cycles*, *10*, 693-709.
Hurtt, G. C., et al. (2006), The underpinnings of land-use history: Three centuries of global gridded land-use transitions, wood harvest activity, and resulting secondary lands, *Global Change Biology*, *12*, 1208-1229.

Juang, J.-Y., et al. (2007), Separating the effects of albedo from eco-physiological changes on surface temperature along a successional chronosequence in the southeastern United States, *Geophysical Research Letters*, *34*, d0i:10.1029/2007GL031296.
Lawrence, D. M., et al. (2007), The Partitioning of Evapotranspiration into Transpiration, Soil Evaporation, and Canopy Evaporation in a GCM: Impacts on Land–Atmosphere Interaction, *Journal of Hydrometeorology*, *8*, 862–880.
Lawrence, P. J. (2004), Climate Impacts of Austrailan Land Cover Change, Ph.D thesis, 240 pp, University of Queensland, Brisbane.
Lawrence, P. J., and T. N. Chase (2007), Representing a MODIS Consistent Land Surface in the Community Land Model (CLM 3.0), *Journal of Geophysical Research*, *112*, G01023 01010.01029/02006JG000168.
Lawrence, P. J., and T. N. Chase (2009), Climate Impacts of Making Evapotranspiration in the Community Land Model (CLM3) Consistent with the Simple Biosphere Model (SiB), *Journal of Hydrometeorology*, *10*, 374-394.
Lean, J., and D. A. Warrilow (1989), Simulation of the regional climatic impact of Amazon deforestation, *Nature*, *342*, 411-413.
Lee, E., et al. (2009), Effects of irrigation and vegetation activity on early Indian summer monsoon variability, *International Journal of Climatology*, *29*, 573-581.
Lee, J.-E., et al. (2005), Root functioning modifies seasonal climate, *Proceedings of the National Academy of Sciences*, *102*, 17576-17581.
Leuning, R., et al. (2005), Carbon and water fluxes over a temperate *Eucalyptus* forest and a tropical wet/dry savanna in Australia: measurements and comparison with MODIS remote sensing estimates, *Agricultural and Forest Meteorology*, *129*, 151-173.
Liang, S., et al. (2002), Validating MODIS land surface reflectance and albedo products: methods and preliminary results, *Remote Sensing of Environment*, *83*, 149-162.
Lobell, D. B., et al. (2006), Biogeophysical impacts of cropland management changes on climate, *Geophysical Research Letters*, *33*, doi:10.1029/2005GL025492.
Loveland, T. R., et al. (2000), Development of a global land cover characteristics database and IGBP DISCover from 1km AVHRR data, *International Journal of Remote Sensing*, *21*, 1303-1330.
McAlpine, C. A., et al. (2007), Modeling the impact of historical land cover change on Australia's regional climate, *Geophysical Research Letters*, *34*, doi:10.1029/2007GL031524.
Myneni, R., et al. (2002), Global products of vegetation leaf area and fraction absorbed PAR from year one of MODIS data, *Remote Sensing of Environment*, *83*, 214-231.
Neale, R. B., et al. (2008), The Impact of Convection on ENSO: From a Delayed Oscillator to a Series of Events, *Journal of Climate*, *21*, DOI:10.1175/2008JCLI2244.1171.
Niyogi, D., et al. (2002), Hydrological Land Surface Response in a Tropical Regime and a Midlatitudinal Regime, *Journal of Hydrometeorology*, *3*, 39-56.
Oleson, K. W., et al. (2004), Effects of land use change on U.S. climate: Impact of surface datasets and model biogeophysics, *Climate Dynamics*, *23*, 117-132.
Oleson, K. W., et al. (2008), Improvements to the Community Land Model and Their Impact on the Hydrological Cycle, *Journal of Geophysical Research*, *113*.
Pielke, R. A. (2001), Influence of the spatial distribution of vegetation and soils on the prediction of cumulus convective rainfall, *Reviews of Geophysics*, *39*, 151-177.

Pielke, R. A., et al. (2002), The influence of land-use change and landscape dynamics on the climate system: relevance to climate-change policy beyond the radiative effect of greenhouse gases, *Philosophical transactions of the Royal Society of London. Series A, 360*, 1-15.

Pitman, A. J., et al. (2009), Uncertainties in climate responses to past land cover change: first results from the LUCID intercomparison study, *Geophysical Research Letters, 36*, doi:10.1029/2009GL039076.

Polcher, J., and K. Laval (1994), A statistical study of the regional impacts of deforestation on climate in the LMD GCM, *Climate Dynamics, 10*, 205-219.

Ramankutty, N., and J. A. Foley (1999), Estimating Historical Changes in Global Land Cover: Croplands from 1700 to 1992, *Global Biogeochemical Cycles, 13*, 997-1027.

Schaaf, C. B., et al. (2002), First operational BRDF, albedo nadir reflectance products from MODIS, *Remote Sensing of Environment, 83*, 135-148.

Shephard, D. (1968), A two-dimensional interpolation function for irregularly-spaced data, paper presented at 23rd ACM national conference, ACM Press.

Shulka, J., et al. (1990), Amazon deforestation and climate change, *Science, 247*, 1322-1325.

von Randow, C., et al. (2004), Comparative measurements and seasonal variations in energy and carbon exchange over forest and pasture in South West Amazonia, *Theoretical and Applied Climatology, 78*, 5-26.

von Storch, H., and F. W. Zwiers (1999), *Statistical Analysis in Climate Research*, Cambridge University Press, Cambridge, UK.

Wang, J. R., et al. (2009), Impact of deforestation in the Amazon basin on cloud climatology, *Proceedings of the National Academy of Sciences, 106*, 3670-3674.

Zhang, H., et al. (1995), Impacts of Tropical Deforestation. Part I: Process Analysis of Local Climatic Change, *Journal of Climate, 9*, 1497-1517.